iScience

Article

Covalent inhibition of *Plasmodium falciparum* Ubc13 impairs global protein synthesis

Graphical abstract

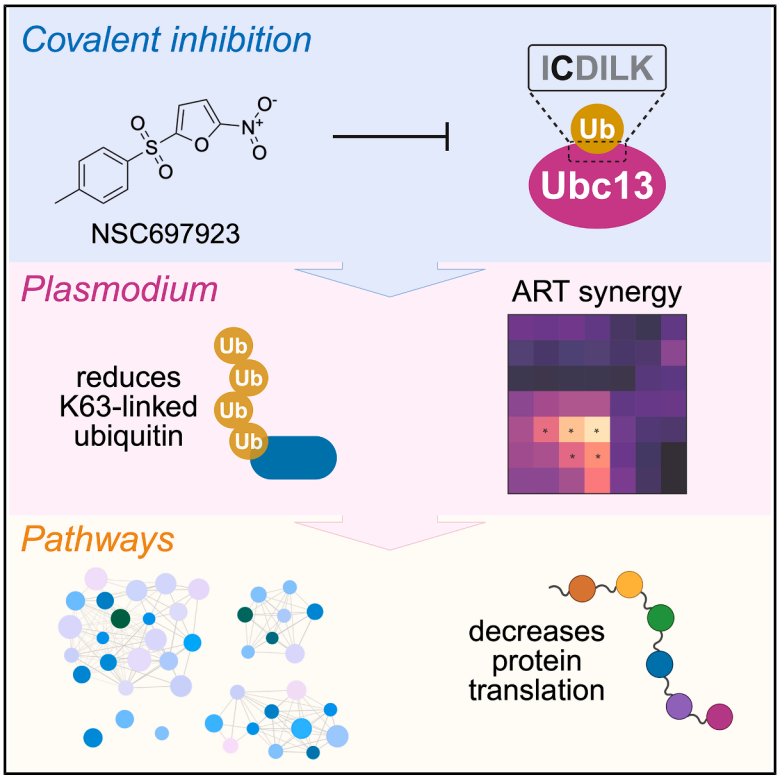

Authors

Anna Truong, Ruitian Hu, Baiyi Quan, ..., Björn F.C. Kafsack, Michael C. Fitzgerald, Emily R. Derbyshire

Correspondence

emily.derbyshire@duke.edu

In brief

Biological sciences; Microbiology; Natural sciences; Pharmacology

Highlights

- NSC697923 covalently modifies the catalytic Cys86 of PfUbc13
- NSC697923 inhibits PfUbc13-ubiquitin *in vitro* and K63-linkages in parasites
- NSC697923 synergizes with the clinical antimalarial drug artemisinin
- Treatment of parasites with NSC697923 attenuates global protein translation

Truong et al., 2025, iScience *28*, 112545
June 20, 2025
https://doi.org/10.1016/j.isci.2025.112545

CellPress

iScience

CellPress
OPEN ACCESS

Article

Covalent inhibition of *Plasmodium falciparum* Ubc13 impairs global protein synthesis

Anna Truong,[1] Ruitian Hu,[1] Baiyi Quan,[1] Morgan A. Bailey,[1] Erin A. Schroeder,[2] Kayla Sylvester,[2] Gaëlle Neveu,[3] Björn F.C. Kafsack,[3] Michael C. Fitzgerald,[1,4] and Emily R. Derbyshire[1,2,5,*]

[1]Department of Chemistry, Duke University, Durham, NC 27708, USA
[2]Department of Molecular Genetics and Microbiology, Duke University Medical Center, Durham, NC 27710, USA
[3]Department of Microbiology and Immunology, Weill Cornell Medicine, New York, NY 10021, USA
[4]Department of Biochemistry, Duke University Medical Center, Durham, NC 27710, USA
[5]Lead contact
*Correspondence: emily.derbyshire@duke.edu
https://doi.org/10.1016/j.isci.2025.112545

SUMMARY

The ubiquitin-conjugating enzyme 13 (Ubc13) has an essential function and putative role in artemisinin activity against *Plasmodium falciparum*. Ubc13 conjugates lysine 63-linked ubiquitin (K63-Ub) to proteins, but the role of this modification in *Plasmodium* remains largely unknown. Herein, we characterize and deploy NSC697923 to interrogate PfUbc13 function. We demonstrate that NSC697923 covalently targets the PfUbc13 catalytic cysteine and exhibits nanomolar inhibitory potency. NSC697923 inhibits multiple life stages and synergizes with the malaria drug dihydroartemisinin. NSC697923 specifically reduces K63-Ub in blood stage parasites, and subsequent chemoproteomic studies identified 31 putative PfUbc13 substrates. These proteins were enriched in transcription, translation, and proteasome processes, and 90% overlapped with previous *Plasmodium* ubiquitinome studies. Nascent protein synthesis was reduced following NSC697923 exposure, supporting a role for PfUbc13 and K63-Ub in mediating protein translation. These findings expand our knowledge of PfUbc13-dependent processes in these pathogenic parasites and highlight this enzyme as a potential antimalarial drug target.

INTRODUCTION

Plasmodium falciparum is the most lethal malaria parasite, responsible for over 90% of the nearly 600,000 malaria fatalities in 2023.[1] Artemisinin (ART)-based combination therapies (ACTs) serve as the World Health Organization's recommended frontline antimalarial treatment.[2] However, the emergence of drug-resistant parasites, notably in Southeast Asia and recently in sub-Saharan Africa, exacerbates the global threat of malaria.[3–8] Thus, there is an urgent need to better understand the mechanism of action of ACTs, and to identify novel antimalarial drug targets. ACTs are active against the clinically symptomatic, asexual blood stage (ABS) of *P. falciparum*.[9,10] During the ABS cycle, the parasite develops into morphologically distinct ring, trophozoite, schizont, and merozoite forms, which are capable of reinvading new blood cells every 48 h.[11] This high replication rate and extensive transformations at this time necessitate mechanisms for precise control of protein expression and function. One such mechanism in *Plasmodium* is ubiquitination, an essential and highly conserved post-translational modification (PTM) that is observed across all eukaryotes.[12]

Ubiquitin (Ub) and ubiquitinated proteins have been detected in all ABS parasite forms.[13] Conjugation of Ub to substrate proteins is catalyzed by highly conserved enzymatic cascades that consist of Ub-activating (E1), Ub-conjugating (E2), and ligase (E3) enzymes.[12,14] This process is initiated by E1-mediated hydrolysis of ATP, adenylation of the Ub C-terminus, and subsequent thioester bond formation at the E1 active site Cys residue.[15] Then, Ub is transferred to the catalytic Cys residue of the E2 through a transthioesterification reaction.[16–18] Finally, through an interaction with an E3 ligase, the Ub is covalently conjugated to a specific protein substrate as a monomer or polyubiquitin chain.[19,20] These Ub chains can be deconstructed and recycled by deubiquitinase (DUB) enzymes.[21,22] Ub chain linkages are defined by the Ub residue to which other Ub monomers are conjugated (i.e., M1, K6, K11, K27, K29, K33, K48, or K63 on Ub), and different linkages coordinate distinct biological functions.[23–25] For example, in well-studied systems, canonical K48-Ub chains mediate 26S proteasomal degradation, whereas K63-Ub linkages are associated with proteasome-independent processes such as DNA repair, signal transduction, and the oxidative stress response, to name a few.[26–33] Polyubiquitination is known to be critical to *Plasmodium*, yet there are many outstanding questions about the identity and function of Ub-signaling pathway members.

A bioinformatic study identified 114 Ub-associated proteins in *P. falciparum*: 8 E1 or E1-like activating enzymes; 14 E2 or E2-like conjugating enzymes; 54 E3 or E3-like ligases, and 29 DUB or DUB-like proteins.[34] Despite the critical role of Ub in the complex *P. falciparum* life cycle, biochemical interrogation

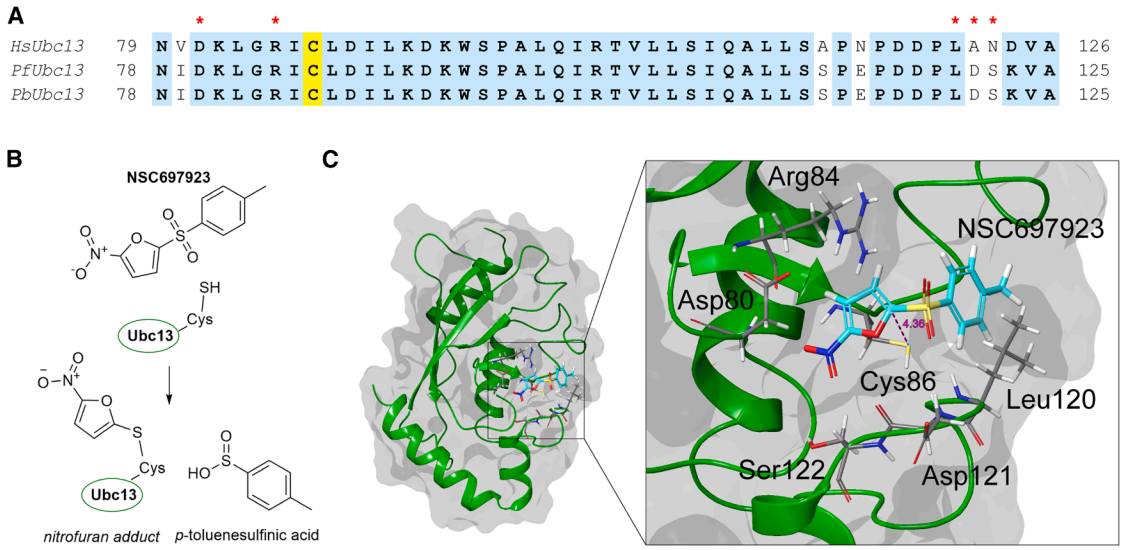

Figure 1. PfUbc13 sequence and structural analysis predicts binding of NSC697923

(A) Multiple sequence alignment of Ubc13 homologs from *H. sapiens*, *P. falciparum*, and *P. berghei* (EMBL-EBI Clustal Omega).[43] Conserved residues (blue) and the catalytic Cys (yellow) is highlighted. Residues previously identified to be important for selectivity of NSC697923 for HsUbc13 are indicated (red star).

(B) Michael-like addition reaction of Ubc13 active site Cys and NSC697923 results in a nitrofuran covalent adduct and *p*-toluenesulfinic acid leaving group.

(C) Docking of NSC697923 (cyan) to PfUbc13 (green, PDB 2R0J). Distance from active site Cys86 (yellow) to the reactive carbon (Michael acceptor) is predicted to be 4.36 Å (magenta) (Schrödinger Maestro).

of these enzymes is sparse, and there are no antimalarial drugs in the pipeline that target this enzyme family. Notably, it was observed that induced genetic knockout of the E2 *P. falciparum* ubiquitin-conjugating enzyme 13 (PfUbc13) sensitizes ABS parasites to dihydroartemisinin (DHA), the therapeutically active drug form of ART, suggesting that PfUbc13 plays a role in recovery from ART-induced damage.[35] Ubc13 mediates K63-Ub chains across eukaryotes, including *P. falciparum,* but the functional consequences of this linkage in parasites remain unknown.[31,36,37] Moreover, PfUbc13 is negatively regulated by the essential protein *P. falciparum* protein kinase 9 (PfPK9) via phosphorylation at Ser106.[38] Confoundingly, chemical inhibition of PfPK9 with the small molecule takinib decreases K63-Ub levels in ABS parasites while increasing liver stage parasite size in the *Plasmodium berghei* rodent malaria model system, though a mechanistic explanation for this size increase remains elusive.[39] PbPK9 is not required for PbUbc13 phosphorylation, and its function appears to be redundant.[40] ABS parasites bearing a PbUbc13 Ser106Ala mutation are not viable, demonstrating that this modification is essential for parasite development.[40] These studies also highlight the advantages of chemically targeting PfUbc13 to further understand the essential role of K63-Ub pathways in *Plasmodium* and the ACT mechanism of action, both of which could reveal new malaria drug targets.[41]

Herein, we integrate chemical biology, biophysical, and biochemical approaches to probe the role of Ubc13 in *Plasmodium* parasites. We first validate NSC697923 binding to PfUbc13 *in vitro*, and then use this molecule to disrupt protein function in parasites.[42] NSC697923 inhibits asexual, liver, and gametocyte parasite stages, and we observe activity against ABS drug-resistant parasite strains and synergy of NSC697923 with DHA. Moreover, we employ NSC697923 to reveal the PfUbc13-dependent K63-Ub landscape, which identified several proteins related to protein translation as potential PfUbc13 substrates. We demonstrate the connection between PfUbc13 and global protein translation using a puromycin-incorporation assay, which suggests PfUbc13-mediation of K63-Ub is involved in the regulation of protein synthesis in *Plasmodium*. More broadly, our data offers numerous potential substrates to better resolve the role of this PTM in *Plasmodium*. Further insights into parasite K63-Ub pathways, especially those implicated in ACT activity, may guide critically needed malaria therapeutic efforts.

RESULTS

Sequence and structural examination of PfUbc13

Sequence alignment of human (Uniprot P61088) and *Plasmodium* Ubc13 (Uniprot *P. falciparum* Q8I3J4, *P. berghei* A0A122ILF4) homologs reveals a high degree of conservation (80% sequence similarity), particularly in the active site that contains the catalytic Cys where Ub-conjugation occurs (Cys86 in *Plasmodium* Ubc13) (Figure 1A). Thus, it was predicted by us and others that NSC697923, an inhibitor of HsUbc13, could be repurposed as a tool to interrogate *Plasmodium* Ubc13 activity.[35,44] NSC697923 was identified as a hit compound in a phenotypic screen designed to discover inhibitors of nuclear factor kappa-B (NF-κB) activation through protein kinase C pathways, but not tumor necrosis factor-alpha (TNF-α) pathways, for the treatment of diffuse large B-cell lymphoma. Subsequent *in vitro* ubiquitination assays revealed that NSC697923 selectively inhibited HsUbc13-mediated polyubiquitin chain synthesis, but not HsUbcH5c polyubiquitin chain synthesis.[44] Since this discovery, its activity and specificity in human cells have been evaluated in several studies.[45–48] NSC697923 covalently

modifies the HsUbc13 active site Cys87 through a Michael-like addition to form a nitrofuran adduct (Figure 1B).[42] Previous studies have identified key residues in a unique cleft adjacent to the catalytic site that impart selectivity of NSC697923 for HsUbc13 over other human E2 enzymes, which include Asp81, Arg85, Leu121, Ala122, and Asn123 (Figure 1A, red stars).[42] Notably, the former three residues are conserved in *Plasmodium* Ubc13 homologs. To assess potential binding, NSC697923 was docked to the PfUbc13 crystal structure (PDB 2R0J) using Maestro by Schrödinger (Figure 1C). Our model predicts that the putative reactive carbon (Michael acceptor) of NSC697923 is within the reaction sphere of the PfUbc13 active site Cys86 thiol (4.36 Å).[49,50] Moreover, the two non-conserved PfUbc13 residues Asp121 and Ser122 were not observed to occlude binding.

To assess potential specificity, we examined the sequences of all putative *Plasmodium* E2's. By specifically comparing residues known to be important for NSC697923 binding, we observed that only PfUbc13 has a high overlap (Figure S1A). The experimentally validated non-NSC697923 binding human E2 HsUbcH5c (Uniprot P61077) was also included in this analysis, and 12 *Plasmodium* E2's had lower overlap than this non-binding control.[44] We also completed an *in silico* screen to evaluate the 14 *Plasmodium* E2's for their potential to bind to NSC697923 (Figure S1B). We found that PfUbc13 is the most similar to HsUbc13 (i.e., highest cleft conservation and lowest C-alpha RMSD), and our docking model of NSC697923 to the PfUbc13 active site is predicted to have the most favorable free energy of binding value (i.e., lowest MM/GBSA). The non-binding HsUbcH5c was again evaluated as a control, where all but 2 *Plasmodium* E2's had MM/GBSA values lower (more favorable predicted binding) than the control and its homolog in *Plasmodium* (Uniprot Q8I607). Only PfUbc13 scored favorably in both analyses to predict NSC697923 binding. Altogether, our *in-silico* analyses suggest that NSC697923 can bind to PfUbc13 with limited predicted binding to other E2's, which supports experimental data in human cells demonstrating NSC697923 specificity toward Ubc13. Hence, experimental validation of NSC697923 binding to PfUbc13 was pursued.

NSC697923 is a covalent inhibitor of PfUbc13

To probe the predicted covalent binding of NSC697923, recombinant HsUbc13, PfUbc13, and a PfUbc13^{C86S} mutant were expressed in *E. coli* and purified to homogeneity (Figure S2A) for high-resolution mass spectrometry (HRMS) analysis. Briefly, protein was incubated with NSC697923 or the DMSO vehicle control, and the resulting extracted-ion chromatograms (EICs) generated from the peptide fragments following trypsin-digestion were examined. This analysis confirmed HsUbc13 Cys87-nitrofuran adduct formation in the NSC697923-treated protein when compared to the DMSO treatment (Figure S2B). PfUbc13 was then similarly treated and analyzed. In the DMSO control sample, we observed a major peak corresponding to the mass (m/z = 817.4852 Da) of the PfUbc13 Cys86 peptide (ICLDILK) (Figure 2A, bottom black trace). A minor peak at a higher retention time was also observed in both the DMSO-treated PfUbc13 and HsUbc13 EICs. Upon incubation with NSC697923, we observed a peak corresponding to the predicted +112.01 Da mass shift (m/z = 929.4952 Da) of the Cys86-nitrofuran adduct (Figure 2A, top blue trace), which was not observed in the DMSO control. Additionally, no unmodified peptide peak was observed, indicating saturation at the active site. In contrast, analysis of the active site mutant PfUbc13^{C86S} following incubation with DMSO or NSC697923 only yielded the mass (m/z = 801.4192) of the unmodified peptide (ISLDILK) in either sample (Figure 2B, black traces) with no detection of a +112.01 Da mass shift (Figure 2B, red traces). Altogether, these data demonstrate that NSC697923 covalently modifies PfUbc13 at the active site Cys86.

To assess NSC697923 inhibition of PfUbc13 Ub-conjugation, *in vitro* Ub transfer assays were performed, and formation of the PfUbc13∼Ub conjugate was monitored by anti-Ub western blot. As Ub activation is necessary for E2∼Ub conjugation to occur, recombinant full-length E1 PfUBA1 (Uniprot Q8I5F9) was expressed and purified to homogeneity (Figure S2A). With incubation of PfUbc13 and PfUBA1 in the presence of Ub, the PfUbc13∼Ub conjugate was observed at 26 kDa (i.e., PfUbc13 18 kDa + Ub 8 kDa) by anti-Ub western blot. There was a dose-dependent inhibition of this band with increasing NSC697923 concentrations (Figure 2C, left) such that no PfUbc13∼Ub conjugate was observed at 64 μM. Assays performed with the PfUbc13^{C86S} mutant revealed no E2∼Ub formation with or without 64 μM NSC697923, further confirming the catalytic role of Cys86 in PfUbc13 Ub-conjugation activity (Figure 2C, right). NSC697923-dependent inhibition was also observed in the HsUbc13 control reactions (Figure S2C). To quantitatively evaluate NSC697923 inhibition of PfUbc13, a fluorescence polarization (FP) assay was employed to measure transfer of the fluorescent tracer fluorescein-Ub (f-Ub) from PfUBA1 to PfUbc13.[51,52] FP is observed when f-Ub is bound to PfUBA1 (132 kDa), and this signal decreases when f-Ub is bound to PfUbc13 (18 kDa). Reduction in f-Ub conjugation to PfUbc13, corresponding to an increase in FP signal and increase in percentage of f-Ub bound to PfUBA1, was observed with NSC697923 addition. In FP assays employing PfUbc13^{C86S} and HsUBA1, only FP signal corresponding to the E1∼Ub conjugate was observed, confirming that the mutant protein does not bind Ub (Figure S2D). Dose-response curves were generated for human and PfUbc13 using the FP assay and fit to calculate the apparent inhibitory constants (K_i) of 0.28 ± 0.07 and 0.36 ± 0.11 μM, respectively (Figure 2D). Overall, a molecule that covalently targets PfUbc13 and inhibits Ub transfer from PfUBA1 with nanomolar potency was identified, thus providing a tool compound to functionally interrogate PfUbc13 in parasites.

NSC697923 exhibits multistage activity and synergizes with DHA

Antiparasitic activity of PfUbc13-chemical inhibition by NSC697923 was assessed during the *Plasmodium* asexual, gametocyte, and liver stages. First, ABS parasite viability was assessed by the nuclear stain SYBR Green.[53,54] NSC697923 inhibited all tested ABS *P. falciparum* parasite strains: drug-sensitive strain 3D7 and drug-resistant strains Dd2 (chloroquine (CQ), pyrimethamine (PYR), mefloquine (MEF)), Dd2_R539T (CQ, PYR, MEF, ART), and W2 (CQ, PYR, MEF). The half-maximal parasite inhibition effective concentrations (EC_{50} values) assessed at the

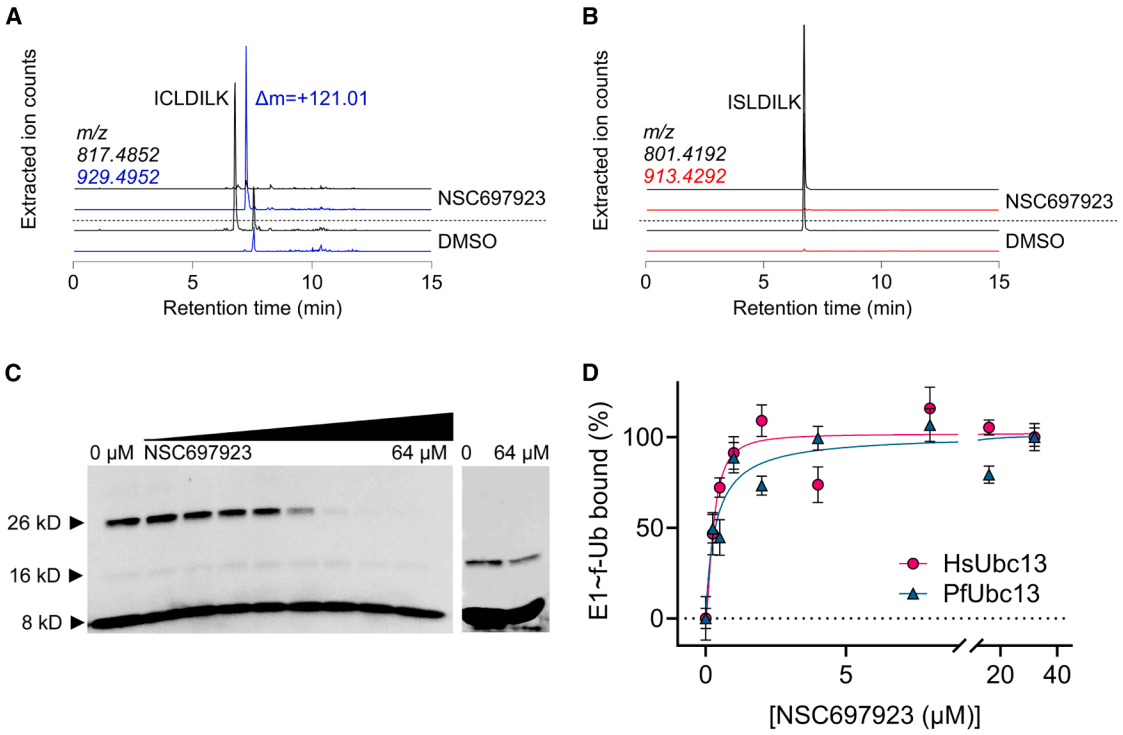

Figure 2. NSC697923 covalently modifies Cys86 and inhibits PfUbc13 activity

(A) LC-HRMS analysis of PfUbc13 with DMSO or NSC697923. Shown are extracted ion chromatograms at the indicated *m/z* with a 5-ppm window. Black traces were monitored at *m/z* for the peptide ICLDILK ($[M + H]^+$ = 817.4852). Blue traces were monitored at *m/z* for the ICLDILK-nitrofuran adduct ($[M + H]^+$ = 929.4952). Data shown are representative of two independent experiments.

(B) LC-HRMS analysis of PfUbc13^{C86S} with DMSO or NSC697923. Shown are extracted ion chromatograms at the indicated *m/z* with a 5-ppm window. Black traces were monitored at *m/z* for the peptide ISLDILK ($[M + H]^+$ = 801.4192). Red traces were monitored at *m/z* for the ISLDILK-nitrofuran adduct ($[M + H]^+$ = 913.4292). Data shown are representative of two independent experiments.

(C) Anti-Ub western blot displays [NSC697923]-dependent inhibition of PfUbc13∼Ub conjugate formation at 26 kDa (right). No conjugate is formed with PfUbc13^{C86S} (left). Bands at 8 and 16 kDa correspond to ubiquitin and di-ubiquitin, respectively. Data shown are representative of two independent experiments.

(D) Inhibition curves generated from fluorescence polarization assay measuring accumulation of fluorescein-Ub conjugated to PfUBA1 upon addition of NSC697923. Inhibitory potency (apparent K_i) of NSC697923 against human (pink) and *P. falciparum* (green) Ubc13 were calculated to be 0.28 ± 0.07 and 0.36 ± 0.11 μM, respectively. Data shown as means ± SEM, $n = 2$.

trophozoite stage were 2.3 ± 0.11, 2.3 ± 0.09, 2.4 ± 0.23, and 1.9 ± 0.13 μM, respectively (Figure 3A), displaying no significant change in potency against drug-sensitive 3D7 and the three tested drug-resistant strains (Figure S3A). A hemolysis assay showed no appreciable RBC toxicity with up to 25 μM NSC697923 over 72-h treatment, demonstrating inhibition was not due to host cell toxicity (Figure S3B).

NSC697923 anti-gametocyte activity was also investigated. Early gametocyte viability was determined based on the intensity of the fluorescent gametocyte reporter tdTomato, which is driven by the *peg4* promoter that becomes active during the treatment window for early gametocytes. For late gametocyte viability, the mitochondrial membrane potential was assessed by DilC1(5)+ staining.[55,56] Treatment of early and late gametocytes with 1 μM NSC697923 resulted in 12% and 21% inhibition, respectively, whereas treatment with 10 μM NSC697923 resulted in 89% and 83% inhibition, respectively (Figure 3B).

To assess liver stage inhibition, we employed the commonly used *P. berghei* rodent malaria liver stage model. In this model, liver stage parasite load is assessed by a luciferase reporter that uses the *eef1a* promoter to drive protein expression. Concurrently, HepG2 hepatocyte viability is assessed by a commercially available kit that measures protease activity with a fluorogenic peptide substrate as a biomarker of cell viability.[57] PfUbc13 is 90% identical to *P. berghei* Ubc13, so it is expected that NSC697923 binds to both proteins (Figure 1A). NSC697923 inhibited liver stage parasites with an EC_{50} value of 8.8 ± 5.2 μM, similar to the observed ABS potency. HepG2 cytotoxicity was observed for NSC697923 at high concentrations, but it did not significantly inhibit HepG2 viability at 12.5 μM (p = 0.5576, Figure S3C). Moreover, based on a microscopy analysis, NSC697923 treatment significantly decreased the size of *P. berghei* liver stage exoerythrocytic forms (EEFs) at 5 μM (Figure S3D).

We sought to characterize the anti-parasitic effect of cotreatment of DHA (EC_{50} = 0.19 ± 0.03 nM, Figure S4A) and the PfUbc13 inhibitor NSC697923. The testing of this specific combination was motivated by the observation that genetic disruption of PfUbc13 sensitizes ABS parasites to DHA; thus, we hypothesized a synergistic interaction would be observed.[35] To evaluate their potential synergy, the observed drug combination

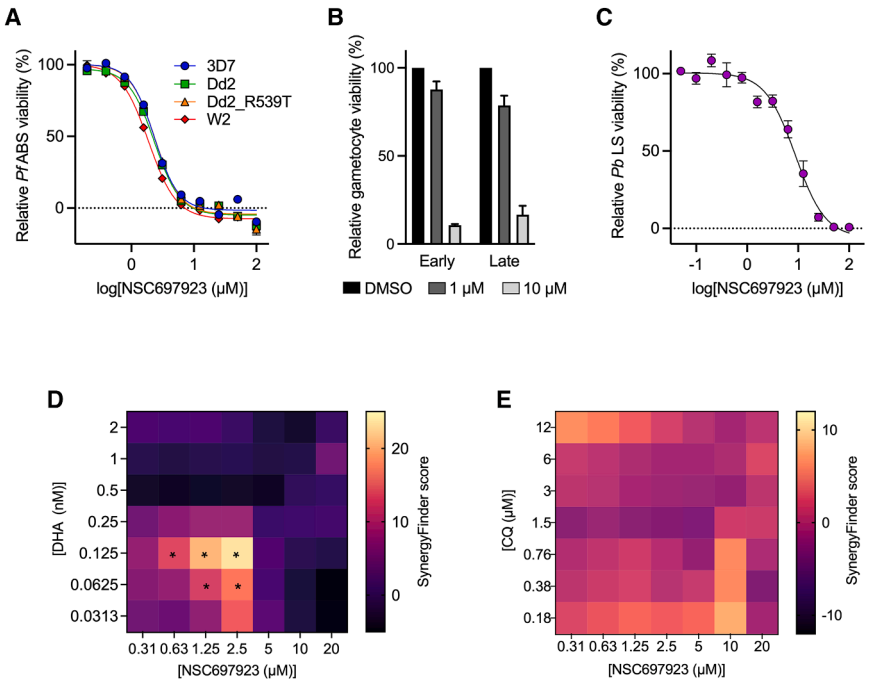

Figure 3. NSC697923 is active against asexual, gametocyte, and liver stage parasites, and specifically synergizes with DHA

(A) NSC697923-dependent inhibition of *P. falciparum* asexual blood stage parasite strains, assessed via the SYBR Green assay: 3D7 (blue, EC_{50} = 2.3 ± 0.11 μM), Dd2 (green, EC_{50} = 2.3 ± 0.09 μM), Dd2_R539T (orange, EC_{50} = 2.4 ± 0.23 μM), and W2 (red, EC_{50} = 1.9 ± 0.13 μM). Data shown as means ± SEM, n = 4.

(B) NSC697923-dependent inhibition of early and late *P. falciparum* gametocyte stage parasites at 1 μM (dark gray) and 10 μM (light gray) relative to DMSO-treatment (black), EC_{50} < 10 μM for both stages, assessed via tdTomato fluorescence or mitochondrial membrane potential, respectively. Data shown as means ± SEM, n = 3.

(C–E) (C) NSC697923-dependent inhibition of *P. berghei* liver stage parasites, assessed via luciferase reporter (EC_{50} = 8.8 ± 2.6 μM). Data are shown as means ± SEM, n = 4. Drug combination responses from (D) cotreatments of DHA (0–2 nM) and NSC697923 (0–20 μM) for *P. falciparum* 3D7 and (E) cotreatments of CQ (0–12 μM) and NSC697923 (0–20 μM) for *P. falciparum* W2 asexual blood stage parasite inhibition calculated with the zero-interaction potency (ZIP) model using SynergyFinder 3.0 with baseline correction. A score of less than −10, between −10 and 10, and greater than 10 indicates that the interaction is antagonistic, additive, or synergistic, respectively. Synergistic interactions are marked with an asterisk (*). Data shown as means, n = 3.

responses were analyzed using SynergyFinder, which uses comparisons with expected combination responses calculated by means of synergy scoring models. The summary synergy scores (i.e., average excess response due to drug interactions) were calculated where a score of less than −10, between −10 and 10, and greater than 10 indicates that the interaction is antagonistic, additive, or synergistic, respectively. Our data indicates synergistic effects at sub-EC_{50} cotreatments of DHA with NSC697923, suggesting that inhibition of PfUbc13 enhances DHA anti-parasitic activity (Figures 3D and S4B). We also assessed cotreatments of CQ with NSC697923 against CQ-resistant W2 ABS parasites. W2 resistance to CQ was verified, displaying a 30-fold loss in sensitivity when compared with CQ-sensitive 3D7 (EC_{50} = 1.00 ± 0.02 μM and 29.4 ± 0.3 nM, respectively). In W2 ABS parasites, we did not observe a synergistic interaction at any tested concentration of CQ and NSC697923 (Figures 3E, S4C, and S4D). Together, these data highlight a specific connection between PfUbc13 and ART pathways.

Characterization of the PfUbc13-dependent K63-ubiquitin landscape

We employed NSC697923 as a tool to elucidate the PfUbc13-dependent K63-Ub landscape in ABS parasites. The in-cell targeting of PfUbc13 K63-Ub conjugation activity by NSC697923 was first assayed in *P. falciparum* 3D7 ABS parasites by western blot using antibodies specific for K63-Ub or K48-Ub linkages (Figures S5A and S5B). We aimed to impact K63-Ub levels in *Plasmodium* without significant toxicity. Therefore, parasites were treated with 1 μM NSC697923 for 48 h, which is below the 72-h 3D7 ABS EC_{50} (2.3 μM) and displayed no significant reduction in viability (Figure S5C). With this treatment, parasites exhibited a significant reduction in K63-Ub levels (20%, p = 0.0322) when compared to the DMSO control, monitored by anti-K63-Ub western blot. A similar analysis of K48-Ub levels showed no statistically significant change (Figures 4A–4D). This reduction in K63-Ub but not K48-Ub levels is consistent with a previous study that observed depletion of K63-Ub levels upon genetic disruption of PfUbc13.[35]

To identify parasite proteins with K63-Ub modification, a label-free quantitative proteomics approach was used. Briefly, ABS parasites were cultured with DMSO or 1 μM NSC697923 for 48 h at the early trophozoite stage, the treatment conditions used in the western blot assay (Figures S5C and S6A). Cells were harvested, parasites were separated from red blood cells, and then these parasites were lysed. *Plasmodium* proteins with K63-Ub modifications were then pulled down from parasite lysate using K63-Ub Tandem Ubiquitin Binding Entities (TUBEs) resin (Figure S6B). TUBEs are polyubiquitin affinity matrices composed of engineered Ub-associated domains that exhibit high specificity for specific linkage types.[58,59] After elution using 50 mM TEAB with 5% SDS and heating at 100°C for 10 min, the sample was submitted to a bottom-up proteomics experiment using an LC-MS/MS readout. Pull-downs with control beads were also completed to assess non-specific binding in both the treated and untreated samples. Quantitative differential analysis of the proteins identified in the DMSO versus NSC697923-treated parasite samples was performed using the data generated in two biological replicates (Tables S1 and S2). Of note, many tryptic peptides report on a single protein, and there was limited coverage of diGly modifications (marker for Ub attachment site) in our workflow. From our analysis, 31

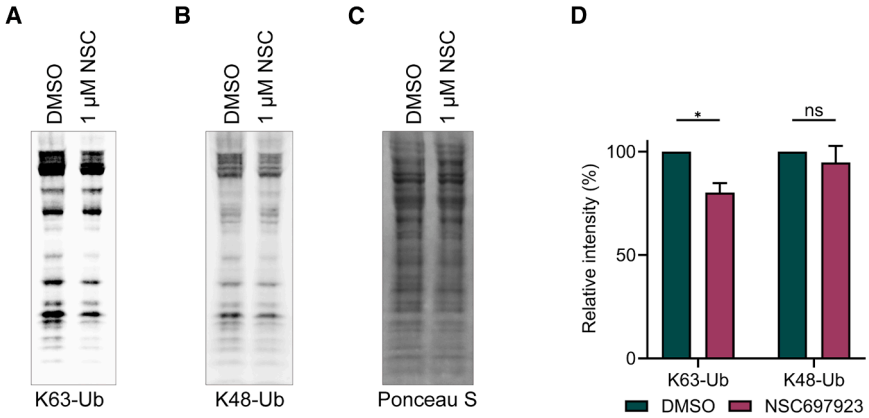

Figure 4. NSC697923 treatment of asexual blood stage *P. falciparum* 3D7 significantly decreases K63-Ub but not K48-Ub levels

(A and B) (A) K63-Ub and (B) K48-Ub were detected and visualized by western blot in NSC697923-treated and DMSO-treated (48 h) asexual blood stage *P. falciparum* 3D7 parasites. (C) Ponceau S measuring total protein was used as a loading control. (A–C) Data shown is representative of three independent experiments.

(D) Quantification of relative K63-Ub and K48-Ub signal intensities in parasites treated with 0.1% DMSO or 1 μM NSC697923. Signals were quantified and normalized to Ponceau S total protein stain (ImageJ). Data shown as means ± SEM, n = 3. * <0.05, not significant (ns) > 0.05; paired t-test.

proteins enriched (-log2 fold-change >0.50) in NSC697923-treated samples that did not nonspecifically bind to the resin in both biological replicates were identified as K63-Ub modified proteins (Figures S6C and S6D, Tables S3A and S3B). From this hit list, a Gene Ontology (GO) network analysis was performed to gain insights into pathways that involve PfUbc13 and proteins modified with K63-Ub (Figure 5A). Several of these GO terms were related to translation, transcription, and proteasome pathways, suggesting that K63-Ub has a role in regulating parasite protein synthesis and degradation processes. We compiled the top 20 highest-confidence GO terms (p-value <0.05) and noted the frequency at which these terms appeared in our 31-protein hit list (Figure 5B). Notably, 4 of the 31 proteins were eukaryotic translation initiation factors (eIFs) (Uniprot Q8IKF0, Q8ILY9, Q8IAZ3, and O97266), suggesting that PfUbc13 has a functional role in mediating the K63-Ub status of these proteins to regulate translation initiation in the parasite. One ribosome protein (Uniprot Q8IM10) was also included among the high confidence hits, further supporting a role for PfUbc13 in effecting parasite protein translation processes.

As an initial means to increase confidence in our protein hits, they were compared to three previously published proteomic datasets of Ub-modified (all linkage types) *P. falciparum* proteins (Figure 5C; Table S3C).[13,60,61] Of note, these other studies were expected to have a significantly higher number of hits as they did not focus on the K63-Ub modification. This comparative analysis yielded a subset of 9 proteins that overlapped in all three studies (Figure 5D). These 9 proteins are taken to be the highest-confidence, putative PfUbc13 substrates modified with K63-Ub, where the site of Ub modification has been identified in each.[61] Excitingly, eIF4A was identified in all four studies, highlighting the putative connection between Ubc13 activity and translation (Figure 5D).

Inhibition of PfUbc13 attenuates global protein translation

We sought to validate the link between PfUbc13 K63-Ub conjugation activity and parasite protein translation. To measure translation, ABS parasites were incubated with O-propargyl puromycin (OPP), a puromycin alkyne analog that can be incorporated into growing translated peptide chains to measure nascent protein synthesis. Subsequent bioconjugation by copper(I)-catalyzed azide-alkyne cycloaddition with AzideFluor488 (AF488) allows for monitoring of protein translation levels via in-gel fluorescence. As a positive control, *P. falciparum* 3D7 trophozoites were treated with the translation inhibitor bruceantin (EC_{50} = 4.5 ± 0.3 nM, Figure S7A) for 4 h and then incubated with OPP for 2 h to assess translation.[62] Bruceantin (5 nM) significantly reduced OPP incorporation (~70%) when compared to the DMSO control (Figures S7B–S7E).[62] We then treated parasites with increasing concentrations of NSC697923 under the same OPP assay conditions. NSC697923 significantly decreased the levels of OPP-incorporation in a dose-dependent manner (Figures 6A and 6B). In contrast, treatment with the negative control drug WR99210 (ABS EC_{50} = ~0.1 nM),[63–65] an inhibitor of the parasite dihydrofolate reductase, did not impact levels of OPP-incorporation (Figures 6C and 6D).[66,67] Protein loading was normalized to Coomassie total protein stain, and ABS parasite viability, assessed via the SYBR Green assay, was not affected by assay conditions (Figures S8A–S8D). As another control, we assessed the impact of heat stress, which is a known stressor throughout the *Plasmodium* life cycle, on global protein translation. In eukaryotes, heat stress results in global repression of protein synthesis as an adaptive response to minimize thermally induced proteome-wide damage.[68–71] Accordingly, we observed that exposure of ABS parasites to 42°C heat stress for 4 h resulted in a significant global reduction of protein synthesis without impacting parasite viability (Figures S9A–S9D). Overall, our data demonstrates that inhibition of PfUbc13 K63-Ub conjugation activity attenuates parasite protein synthesis, suggesting that K63-Ub has a role in the regulation of translation in malaria parasites.

DISCUSSION

Ub is critical for progression of the malaria parasite life cycle at every life stage.[13] Further, Ub pathways are involved in the modes of action of frontline antimalarial drugs and parasite drug resistance, highlighting its relevance to malaria drug treatment options.[9,10,72] However, these pathways are largely unresolved, and parasite Ub enzymes remain underexplored as potential antimalarial drug targets.[73] Of particular interest is

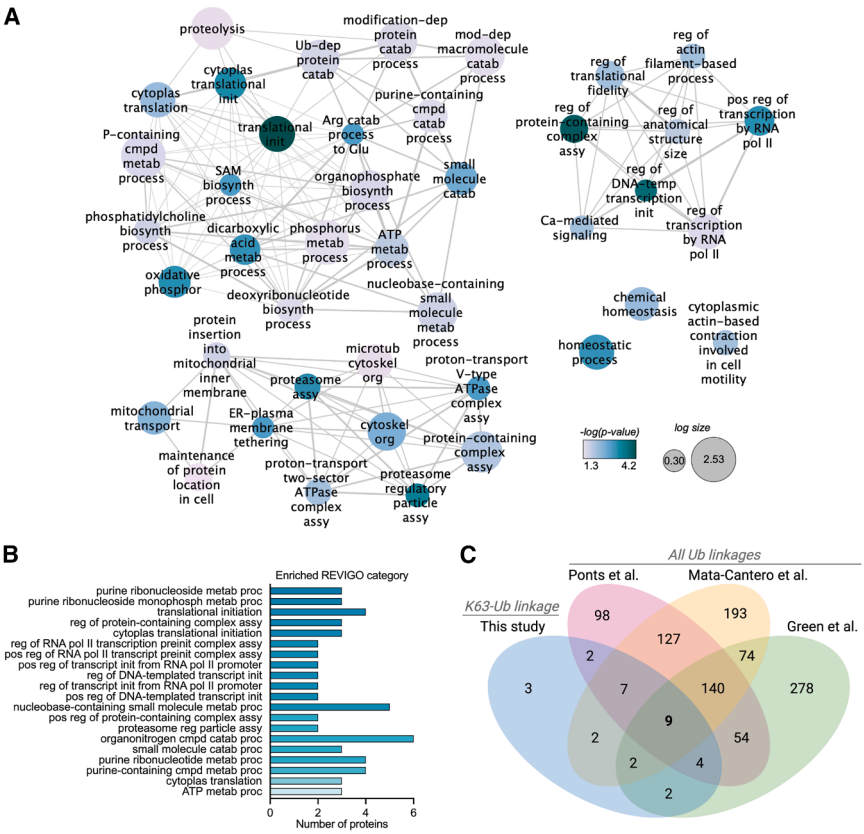

D

Uniprot ID	PlasmoDB ID	Gene name	PlasmoDB descriptor
Q8II60	PF3D7_1130400	RPT5	26S protease regulatory subunit 6A, putative
Q8IKF0	PF3D7_1468700	eIF4A	eukaryotic initiation factor 4A
Q8IKF6	PF3D7_1468100	MORC	MORC family protein
Q8IDQ9	PF3D7_1343000	PMT	phosphoethanolamine N-methyltransferase
Q8IHY0	PF3D7_1138500	PPM2	protein phosphatase PPM2, protein phosphatase 2C
Q8IL94	PF3D7_1437200	N/A	ribonucleoside-diphosphate reductase large subunit, putative
Q7K6A4	PF3D7_0922200	SAMS	S-adenosylmethionine synthetase
Q8I5F9	PF3D7_1225800	UBA1	ubiquitin-activating enzyme E1
Q8IL71	PF3D7_1439800	N/A	vesicle-associated membrane protein, putative

Figure 5. Proteomic characterization of the PfUbc13-dependent K63-Ub landscape in asexual blood stage parasites

(A) Gene ontology (GO) enrichment mapping detailing biological processes of 31 protein hits (shown are curated GO terms with p-value <0.05; Fisher's exact test). GO terms are denoted by nodes. Node color represents the significance of the enriched annotations, and the node size represents the number of annotations for the GO term in the database for *P. falciparum*. Highly similar GO terms are linked by edges in the graph, where the line width indicates the degree of similarity. Map generated in REVIGO (Reduce + Visualize Gene Ontology) and visualized in Cytoscape.

(B) Top 20 significantly enriched GO terms (p-value <0.05, Fisher's exact test) were compiled, and number of proteins (X axis) of the specific GO term from the 31 hit proteins was visualized (magnitude of p-value is indicative of Y axis placement and color transparency).

(C) Overlap of 31 enriched proteins with -log2 fold-change >0.50 identified in two independent experiments (i.e., decreased K63-Ub modification in NSC69723-treated parasites) with three previous datasets identifying total ubiquitinated parasite proteins (i.e., all linkage types).

(D) Compiled identifiers and descriptions of nine proteins observed with ubiquitin modification in this study and three others. See also Tables S1, S2, and S3.

PfUbc13, an enzyme expressed throughout the asexual, sexual, and liver stages of *Plasmodium*. PfUbc13 is known to be essential for the parasite ABS, and with putative involvement in ART antimalarial activity.[35,41,74–76] Ubc13 homologs in well-characterized systems have been shown to be central mediators in the specific attachment of K63-Ub chains, which intriguingly regulate proteasome-independent processes such as DNA repair, protein localization, endo-lysosomal pathways, and other critical cellular functions. However, knowledge of Ubc13 and K63-Ub from higher eukaryotes does not always translate directly to *Plasmodium*, whose ~5,300 protein-coding genes widely diverge from humans and model organisms. For example, Ubc13 in humans ubiquitinates TNF receptor-associated factor (TRAF)-family adapter proteins and NF-κB essential modulator (NEMO), which are key signaling molecules in immune and inflammatory responses; however, *Plasmodium* does not express TRAF proteins or NEMO. Beyond that, *Plasmodium* lacks complex, canonical immune pathways that are observed in higher eukaryotes.[28,77,78] These divergences demonstrate the need for focused studies on Ubc13 and atypical K63-Ub linkages in *Plasmodium*.

To enhance our functional understanding of PfUbc13 and K63-Ub in malaria parasites, we first sought to identify a chemical inhibitor. Having observed a high degree of sequence and structural conservation between human and *P. falciparum* Ubc13 homologs (80%), it was hypothesized that the known covalent HsUbc13 inhibitor NSC697923 would also bind to PfUbc13. Indeed, mass spectrometry confirmed NSC697923 covalently modifies recombinant PfUbc13, but this reaction does not occur when the catalytic cysteine (Cys86) is mutated, confirming the binding site. Furthermore, we observed NSC697923-dependent inhibition of *in vitro* Ub transfer from the E1 PfUBA1 to PfUbc13 with nanomolar potency (K_i). Examination of the HsUbc13-NSC697923 cocrystal structure (PDB 4ONM) and the PfUbc13 crystal structure (PDB 2R0J) suggests that even more selective inhibitors for the parasite homolog can be generated, with NSC697923 as a promising starting point. Importantly, extensive structure-activity relationship studies of NSC697923 are needed to generate a species selective PfUbc13 inhibitor to improve the therapeutic index (HepG2 CC_{50} = 30.0 μM, ABS selectivity index = 13.0) and identify a suitable antimalarial lead compound. Notably, residues Ala122 and Asn123 in the active site of HsUbc13 are not conserved in the *Plasmodium* homolog (Asp121 and Ser122, respectively), providing variation that may be exploited in

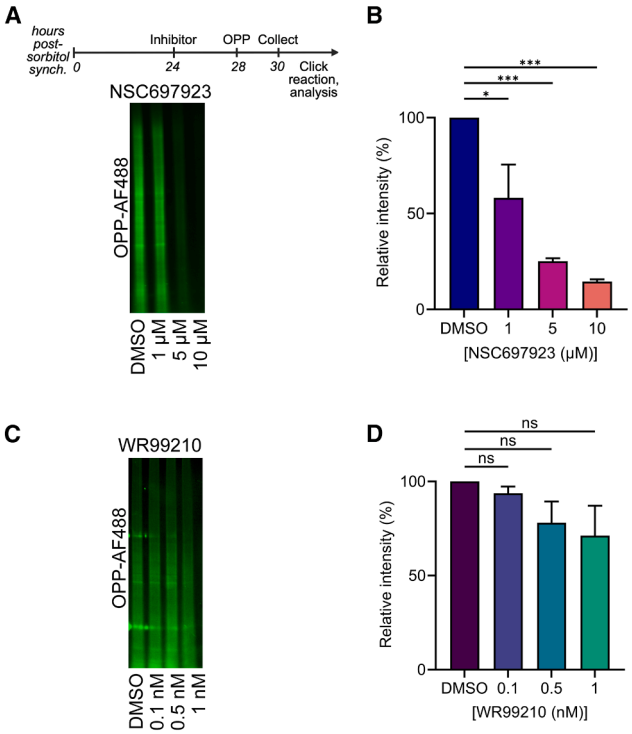

Figure 6. NSC697923-treatment reduces parasite global nascent protein translation

(A–D) Protein incorporation of OPP (2-h) following (A) NSC697923 or (C) WR99210 (4-h) treatment is monitored by Cu(I)-catalyzed click reaction with AF488 and visualized by in-gel fluorescence. Representative gels are shown from three independent experiments. Quantification of AF488 fluorescent signal upon (B) NSC697923- or (D) WR99210-treatment relative to DMSO. Data shown as means ± SEM, n = 3. * <0.05, *** <0.005, not significant (ns) > 0.05; one-way ANOVA, Dunnett's multiple comparison.

medicinal chemistry efforts. As covalent targeting of the PfUbc13 catalytic Cys86 was observed to inhibit its activity, screening of electrophilic, Cys-targeting small molecule libraries is one approach that could yield a more selective and potent PfUbc13 inhibitor, previously achieved in screens against *P. falciparum* ubiquitin C-terminal hydrolase L3.[79–82] Beyond greater species selectivity, experimental studies to support our *in silico* sequence analyses and docking screen of the 14 putative *Plasmodium* E2 enzymes would also be needed to assess specificity. If needed, there is a path to exploit the unique cleft in Ubc13 to achieve greater E2 specificity. Medicinal chemistry efforts are critical next steps to improve these liabilities and further explore PfUbc13 as an antimalarial drug target.

PfUbc13 activity is negatively regulated via phosphorylation of Ser106 by the orphan kinase PfPK9, and chemical inhibition of the mouse model homolog *P. berghei* PK9 results in significantly larger EEF size.[38,39] In contrast, chemical inhibition of Ubc13 in *P. berghei* resulted in smaller parasite forms, suggesting that this enzyme is not linked to the increased EEF size phenotype. Thus, other PK9 substrates are likely to be involved and could be identified in phosphoproteomic studies.[83–88] Additionally, the employment of selective inhibitors of PfPK9 could be implemented with a Ubc13 inhibitor to untangle specific kinase-Ubc13 functions.[89] Moreover, it has been shown that PbPK9 is nonessential to ABS *P. berghei* while the *P. falciparum* homolog is essential.[40,41] Phosphorylated-Ubc13 is detectable even upon conditional knockout of PbPK9, indicating that additional parasite kinases are involved in the regulation of *Plasmodium* Ubc13 activity.[40] The identification of the additional kinases/phosphatases involved in PfUbc13 Ser106 phosphorylation/dephosphorylation would enhance the current understanding of its complex regulation.

To further characterize PfUbc13 as a drug target, we performed resistance profiling against several drug-resistant parasite strains. These results indicate that susceptibility to NSC697923 is unchanged in drug-resistant parasite strains and thus unaffected by CQ, PYR, MEF, and ART resistance pathways. Moreover, assessment of anti-parasitic activity against late gametocytes displayed single micromolar potency (EC_{50}), indicating that inhibition of PfUbc13 could have transmission blocking effects, which could be determined with standard membrane feeding assays to measure the infectivity of gametocyte stage parasites treated with NSC697923. Furthermore, it was previously observed that genetic disruption of *Pfubc13* sensitizes the parasite to DHA.[35] Accordingly, we observed that NSC697923 synergizes with sub-EC_{50} concentrations of DHA, but not with CQ, to inhibit the ABS. This implicates PfUbc13 in the DHA mode of action and suggests that cotreatments of DHA with PfUbc13 inhibitors could serve as a novel avenue to circumvent ART resistance. In contrast, chemical or genetic inhibition of parasite DUBs, which deconstruct Ub chains, is observed to enhance ART anti-parasitic activity, demonstrating the complex effects of Ub signaling on parasite susceptibility to ART therapies.[90–92] Biochemical characterization of members of the family of ovarian tumor domain-containing (OTUD) DUB enzymes in the related apicomplexan parasite *Toxoplasma gondii* has identified several *T. gondii* OTUD DUBs with *in vitro* specificity for K63-Ub linkages.[93] Two of these DUBs, OTUD3A and OTUD3B (TGME49_258780 and TGME49_229710, respectively), have orthologs in *P. falciparum* (PF3D7_0923100 and PF3D7_1031400, respectively).[93] Future investigations could explore if these DUBs have functional conservation in *P. falciparum*, demonstrating that they work in opposition to PfUbc13 to regulate K63-Ub levels. Collectively, these findings highlight the potential for malaria combination therapies that employ ART and PfUbc13 inhibitors.

We pursued proteomic studies to investigate PfUbc13-dependent pathways and the biological functions of K63-Ub in the parasites. Following chemical inhibition of PfUbc13, we pulled down K63-Ub modified proteins from ABS parasites using K63-Ub TUBEs resin and determined proteins that were less abundant following NSC697923 treatment compared to DMSO controls and that did not bind to the negative control resin. These 31 proteins alone serve as much needed starting points to unravel K63-Ub regulated pathways. Our set of 31 hit proteins was utilized in a GO analysis to provide the first insights into the specific biological pathways of PfUbc13-mediated K63-Ub in *P. falciparum*. Notably, our hits included proteasome, ribosome, and translation initiation factor proteins, suggesting that PfUbc13 and K63-Ub have roles in regulating protein expression and abundance through effecting degradation and translation processes.

It remains possible that some identified proteins interact with a PfUbc13 substrate and are thus indirectly pulled down. To enhance confidence in our hits, we next compared the list of predicted PfUbc13 substrates with three proteomic studies that identified *P. falciparum* ubiquitinated proteins.[13,60,61] We anticipated differences in hit identification among the three studies, which could be attributed to notable technical differences, specifically in the Ub enrichment tool (i.e., TUBEs versus antibody), and data acquisition and analysis methods.[94,95] But we also expected some proteins from our study to overlap with the three previous studies and reasoned that these overlapping proteins would be the highest confidence hits. Indeed, we determined 90% overlap with at least one of three datasets (Figure 5C), and 9 proteins were in all four datasets (Figure 5D). While our methodology did not enrich for tryptic peptides that contained the PTM (i.e., post-digestion enrichment), the site of Ub attachment in these 9 proteins was confirmed by Holder et al. Thus, there is strong evidence to support these proteins as direct Ubc13 substrates.

In accordance with our GO analyses, we observed NSC697923-dependent inhibition of OPP-incorporation into nascent proteins of ABS parasites, supporting PfUbc13 mediation of K63-Ub in regulating protein translation. Ribosomes modified with K63-Ub is a hallmark of the oxidative stress response in yeast, thus implicating this function in *Plasmodium*.[29,96] eIFs have also been observed to be modified with Ub, with evidence for K63-Ub modification of eIF2Bϵ; although, the *P. falciparum* homolog (26%) was not identified in our dataset.[97–99] Proteasome subunits have also been observed to be modified with Ub in humans.[100–103] Furthermore, K63-Ub serves as a signal for protein degradation through endolysosomal pathways in humans and plants, but this function remains to be verified in *P. falciparum*.[33,104–107] If this activity is conserved, it would be exciting to consider targeted protein degradation via PfUbc13 recruitment as a novel antimalarial strategy.[108,109]

Our OPP incorporation study further strengthened the proposed role for PfUbc13 in affecting protein translation. We believe that the observed reduction in protein translation with PfUbc13 inhibition is consistent with a prior study showing that genetic disruption of PfUbc13 sensitizes parasites to DNA damage induced by treatment with methyl methanesulfonate. This study also showed that ABS parasites treated with NSC697923 progressed normally to schizonts, but development 49 and 69 h post-invasion was delayed, which phenocopied PfUbc13-deletion.[35] These later stages are when DNA replication, nuclear division, and merozoite differentiation occur, which supports a role for PfUbc13 in maintaining normal DNA replication. DNA damage has been shown to result in global repression of translation in eukaryotes through well-defined pathways: activation of kinases and eIF2α phosphorylation signaling for reduction of protein synthesis, induction of ubiquitination of 40S and 60S ribosomal units resulting in attenuation of ribosome translation activity, among other mechanisms.[110,111] Hence, improper maintenance of DNA through impairment of PfUbc13 would be expected to inhibit protein translation, which was observed in our OPP-incorporation experiments. In fact, 22 of our 31 hit proteins are annotated with nuclear localization by GO cellular component analysis, supporting the role of PfUbc13 in DNA maintenance pathways. Additional experiments assessing parasite DNA damage upon treatment with NSC697923 using terminal deoxynucleotidyltransferase-mediated dUTP-biotin nick end labeling (TUNEL) assays, measuring phosphorylation of *Plasmodium* histone H2A, and/or monitoring the expression levels of DNA repair proteins would further strengthen the possible link between DNA damage and PfUbc13.[112,113]

Moreover, the *Plasmodium* mitochondrion is also translationally active, prompting the question if PfUbc13 has a specific role in regulating mitochondrial translation.[114–116] A previous study using mouse and human cells determined that G-Protein pathway suppressor 2 (GPS2) functions in opposition to Ubc13 to inhibit K63-ubiquitination of several mitochondrial RNA binding and translation proteins, which include PABPC1, RPS1, RACK1 and eIF3M.[46] Although we did not identify the *Plasmodium* orthologs of the GPS2-regulated mitochondrial proteins as hits, three of our hit proteins were predicted by GO cellular component analysis to localize to the mitochondria: PF3D7_1235700, PF3D7_1404100, PF3D7_1368600 (Uniprot Q8I0V2, Q8IM53, Q8ID24, respectively) (Table S3B). Most interesting in the context of mitochondrial translation is PF3D7_1404100 (cytochrome *c*, putative). K63-ubiquitination of human mitochondrial proteins, including cytochrome *c*, has been observed to regulate apoptotic signaling pathways and impact organellar functions, such as translation, implicating this as an intriguing possibility in *Plasmodium*.[117,118] However, human GPS2 shares sequence identity (37%) to an uncharacterized *Plasmodium* protein (Uniprot Q8IIX7) that is predicted to be exported, suggesting that even if this uncharacterized protein is a *bona-fide Plasmodium* GPS2 ortholog, its function and related pathways may not be conserved.[119] Relatedly, in a *Drosophila* study investigating mitochondrial stress mechanisms, the Ubc13 ortholog Ben is required for the stability of PTEN-induced kinase 1 (PINK1), likely through its K63-ubiquitination. PINK1 accumulation to the outer mitochondrial membrane is a hallmark of stressed, damaged mitochondria, and subsequently signals for the degradation of the mitofusin protein Marf as a possible cell-protective response.[120] We identified one *Plasmodium* kinase PF3D7_0321400 (pseudo protein kinase 1, putative; Uniprot C0H482) in our proteomics study, but it shares low sequence identity with PINK1 (20%). PINK1 shares slightly higher sequence identity (~25%) with several *Plasmodium* members of the family of cyclin-dependent kinases; however, to date, no *Plasmodium* kinases have been observed with mitochondrial localization. Regardless, it would be intriguing to evaluate if PfUbc13 has a role in mitochondrial stress pathways, subsequently impacting its functions like translation, by employing NSC697923 and measuring mitochondrial activity.[121,122] However, *Plasmodium* parasites have notably different mitochondrial biology compared to humans and model organisms (e.g., ABS parasites have one mitochondrion while human cells can have thousands; the mitochondrion genome in *Plasmodium* encodes 3 genes versus 37 in humans), so these implications from other systems should be viewed with caution as it is likely that regulation of mitochondrial translation and quality control in *Plasmodium* widely differs from other higher eukaryotes.

Our putative substrate proteins of PfUbc13 are excellent starting points for future biochemical validation studies, but those

experiments require identification of a cognate E3 partner. A recent study identified the E3 PfRBR (PF3D7_0303800) as a cognate partner to PfUbc13 (PF3D7_0527100).[123] Here, we examined a global *P. falciparum* transcriptome dataset and performed a Pearson correlation (PC) analysis of transcript levels of 44 predicted E3 ligases across six parasite developmental stages and compared them to PfUbc13 transcript levels (Figure S10A).[74] It has previously been established that pathway enzymes are co-regulated; thus, we sought to leverage a correlation in transcript levels to identify possible partners.[124,125] Indeed, we determined that PfUbc13 and PfRBR share a PC value of 0.97, the second-highest value in our analysis. There were also three additional putative E3 enzymes that shared a high PC value (>0.90) with PfUbc13: PF3D7_0916400, PF3D7_0502000, PF3D7_1119400. Intriguingly, PF3D7_0916400 was identified as a candidate gene associated with ART susceptibility in *P. falciparum* isolates from Kenya.[126] Additionally, a recent study observed *in vitro* Ub transfer from PfUbc13 to the catalytic domain of the E3 PfHEUL (PF3D7_0826100), which also shared a relatively high PC value (0.85) in our analysis.[127] Of note, the mammalian mitochondrial E3 ligase MUL1 works with Ubc13 to modify mitochondrial RNA binding and translation proteins with K63-Ub linkages.[46] MUL1 shares sequence identity (~35%) with *Plasmodium* members of the family of Really Interesting New Gene (RING) E3 ligases: PF3D7_0627300, PF3D7_0316900, PF3D7_0215100, PF3D7_1013000 (Uniprot Q8I660, O77387, Q8IJR5, C6KTA9, respectively). None have been observed with mitochondrial localization to date, but PF3D7_0316900 also displayed a relatively high PC value (0.85) in our analysis. To experimentally identify cognate E3 partners of PfUbc13 in a cellular context, unbiased activity-based protein profiling (ABPP) approaches could be used.[128–131] Accordingly, once a *Plasmodium* E1-E2-E3 pathway is established, substrate proteins from our proteomic study can also be biochemically validated.[132] Moreover, *in vivo* studies in the parasite can be envisioned leveraging chemical biology crosslinking strategies that have been employed to study Ub cascades by semisynthetic modifications or mutations of these enzymes.[133,134]

Collectively, we show that PfUbc13 can be chemically inhibited via covalent targeting of its catalytic Cys86 by the compound NSC697923. This inhibitor has antiparasitic activity against drug-sensitive and drug-resistant ABS malaria parasites, in addition to liver and gametocyte stages. Notably, treatment with NSC697923 synergizes with DHA anti-parasitic activity. These studies set a path to generate more selective and potent probes, and antimalarial drugs against PfUbc13. We highlight the use of NSC697923 as the first-known chemical probe of PfUbc13 to identify and characterize the K63-Ub proteome of ABS *P. falciparum*, which implicated the enzyme in regulating diverse pathways, including protein translation. Ultimately, we have advanced the foundation for PfUbc13 as a malaria drug target and targeting K63-Ub broadly as a novel therapeutic avenue.

Limitations of the study

Specificity of NSC697923 for PfUbc13 over other *Plasmodium* E2 proteins was assessed using *in-silico* methods, and these results need experimental validation in parasites using chemoproteomic methods, such as thermal proteome profiling or the cellular thermal shift assay, and in *in vitro* biochemical binding assays. Additionally, NSC697923 is not selective for *Plasmodium* Ubc13 over the human ortholog. Thus, structure-activity relationship studies are required to optimize selectivity of NSC697923 for PfUbc13 and to minimize host cytotoxicity. Moreover, our proteomics study had low coverage of diGly modifications, which limited our ability to confirm hits and map the ubiquitination site on the putative substrates. This workflow could employ enrichment with a diGly antibody or usage of more sophisticated data acquisition methods or technologies to determine bona fide K63-Ub modification by PfUbc13. Finally, in-depth studies focused on our proteomic hits, such as mutation of putative ubiquitination sites in *Plasmodium*, would provide mechanistic insights to further support the connection between protein translation in parasites and PfUbc13 activity.

RESOURCE AVAILABILITY

Lead contact

Further information and requests for resources and reagents should be directed to and will be fulfilled by the lead contact, Emily R. Derbyshire (emily.derbyshire@duke.edu).

Materials availability

This study did not generate new unique reagents.

Data and code availability

- The raw mass spectrometry proteomics data have been deposited to the ProteomeXchange Consortium via the PRIDE partner repository with the dataset identifier PXD059643 and are publicly available as of the date of publication.
- Software used herein are available for either download or online usage at the provided online locations noted in the key resources table. This paper does not report original code.
- Any additional information required to reanalyze the data reported in this paper is available from the lead contact upon request.

ACKNOWLEDGMENTS

We thank the University of Georgia SporoCore for providing *P. berghei*-infected *Anopheles stephensi* mosquitos. We are also grateful to the Derbyshire lab for insightful discussions. Schematics were created using BioRender. This research was supported by a NIH R01 AI173295, Sloan Research Fellowship, and a Camille Dreyfus-Teacher Scholar Award to E.R.D. Fellowship support was provided to A.T. by the NSF GRFP (DGE 2139754). We thank Dr. Peter Silinski for mass spectrometry assistance and Dr. Grace Sturrock for uploading the proteomics data.

AUTHOR CONTRIBUTIONS

A.T. performed molecular modeling, mutagenesis, blood stage assays, K63-TUBEs experiments, and puromycin-incorporation assays. A.T. and R.H. performed protein expression and purification and biochemical assays. B.Q., M.A.B., and M.C.F. performed and supported mass spectrometry data acquisition and analysis. A.T., B.Q., M.A.B., and M.C.F. analyzed the proteomics data. E.A.S. and K.S. performed liver stage assays and cytotoxicity testing. G.N. and B.F.C.K. performed gametocyte assays. A.T. and E.R.D. designed the experiments and wrote the manuscript. All authors commented on the manuscript.

DECLARATION OF INTERESTS

The authors declare no competing interests.

STAR★METHODS

Detailed methods are provided in the online version of this paper and include the following:

- KEY RESOURCES TABLE
- EXPERIMENTAL MODEL AND STUDY PARTICIPANT DETAILS
  - Cell lines
  - Parasite lines
  - Bacterial strains
- METHOD DETAILS
  - Molecular modeling
  - Protein expression and purification
  - Mass spectrometry analysis of tryptic peptides
  - Ubiquitin transfer visualized by western blot
  - Fluorescence polarization assay
  - *Plasmodium* blood stage culture
  - *Plasmodium* blood stage inhibition assays
  - *Plasmodium* liver stage inhibition assays
  - *Plasmodium* liver stage size assays
  - *Plasmodium* gametocyte inhibition assays
  - Evaluation of K63-Ub and K48-Ub levels
  - K63-TUBEs enrichment of *Plasmodium* proteins
  - LC-MS/MS analysis
  - Label-free quantitation data processing
  - O-propargyl puromycin incorporation assay
- QUANTIFICATION AND STATISTICAL ANALYSIS

SUPPLEMENTAL INFORMATION

Supplemental information can be found online at https://doi.org/10.1016/j.isci.2025.112545.

Received: October 3, 2024
Revised: March 5, 2025
Accepted: April 24, 2025
Published: April 28, 2025

REFERENCES

1. WHO (2025). World Malaria Report 2024.
2. WHO (2023). WHO Guidelines for Malaria.
3. Ashley, E.A., Dhorda, M., Fairhurst, R.M., Amaratunga, C., Lim, P., Suon, S., Sreng, S., Anderson, J.M., Mao, S., Sam, B., et al. (2014). Spread of artemisinin resistance in Plasmodium falciparum malaria. N. Engl. J. Med. *371*, 411–423. https://doi.org/10.1056/NEJMoa1314981.
4. van der Pluijm, R.W., Tripura, R., Hoglund, R.M., Pyae Phyo, A., Lek, D., Ul Islam, A., Anvikar, A.R., Satpathi, P., Satpathi, S., Behera, P.K., et al. (2020). Triple artemisinin-based combination therapies versus artemisinin-based combination therapies for uncomplicated Plasmodium falciparum malaria: a multicentre, open-label, randomised clinical trial. Lancet *395*, 1345–1360. https://doi.org/10.1016/S0140-6736(20)30552-3.
5. Amaratunga, C., Lim, P., Suon, S., Sreng, S., Mao, S., Sopha, C., Sam, B., Dek, D., Try, V., Amato, R., et al. (2016). Dihydroartemisinin-piperaquine resistance in Plasmodium falciparum malaria in Cambodia: a multisite prospective cohort study. Lancet Infect. Dis. *16*, 357–365. https://doi.org/10.1016/S1473-3099(15)00487-9.
6. Awor, P., Coppée, R., Khim, N., Rondepierre, L., Roesch, C., Khean, C., Kul, C., Eam, R., Lorn, T., Athieno, P., et al. (2024). Indigenous emergence and spread of kelch13 C469Y artemisinin-resistant Plasmodium falciparum in Uganda. Antimicrob. Agents Chemother. *68*, e0165923. https://doi.org/10.1128/aac.01659-23.
7. Balikagala, B., Fukuda, N., Ikeda, M., Katuro, O.T., Tachibana, S.I., Yamauchi, M., Opio, W., Emoto, S., Anywar, D.A., Kimura, E., et al. (2021). Evidence of Artemisinin-Resistant Malaria in Africa. N. Engl. J. Med. *385*, 1163–1171. https://doi.org/10.1056/NEJMoa2101746.
8. Menard, D., Khim, N., Beghain, J., Adegnika, A.A., Shafiul-Alam, M., Amodu, O., Rahim-Awab, G., Barnadas, C., Berry, A., Boum, Y., et al. (2016). A Worldwide Map of Plasmodium falciparum K13-Propeller Polymorphisms. N. Engl. J. Med. *374*, 2453–2464. https://doi.org/10.1056/NEJMoa1513137.
9. Bridgford, J.L., Xie, S.C., Cobbold, S.A., Pasaje, C.F.A., Herrmann, S., Yang, T., Gillett, D.L., Dick, L.R., Ralph, S.A., Dogovski, C., et al. (2018). Artemisinin kills malaria parasites by damaging proteins and inhibiting the proteasome. Nat. Commun. *9*, 3801. https://doi.org/10.1038/s41467-018-06221-1.
10. Tilley, L., Straimer, J., Gnädig, N.F., Ralph, S.A., and Fidock, D.A. (2016). Artemisinin Action and Resistance in Plasmodium falciparum. Trends Parasitol. *32*, 682–696. https://doi.org/10.1016/j.pt.2016.05.010.
11. Venugopal, K., Hentzschel, F., Valkiūnas, G., and Marti, M. (2020). Plasmodium asexual growth and sexual development in the haematopoietic niche of the host. Nat. Rev. Microbiol. *18*, 177–189. https://doi.org/10.1038/s41579-019-0306-2.
12. Komander, D., and Rape, M. (2012). The ubiquitin code. Annu. Rev. Biochem. *81*, 203–229. https://doi.org/10.1146/annurev-biochem-060310-170328.
13. Ponts, N., Saraf, A., Chung, D.W.D., Harris, A., Prudhomme, J., Washburn, M.P., Florens, L., and Le Roch, K.G. (2011). Unraveling the ubiquitome of the human malaria parasite. J. Biol. Chem. *286*, 40320–40330. https://doi.org/10.1074/jbc.M111.238790.
14. Pickart, C.M., and Eddins, M.J. (2004). Ubiquitin: structures, functions, mechanisms. Biochim. Biophys. Acta *1695*, 55–72. https://doi.org/10.1016/j.bbamcr.2004.09.019.
15. Schulman, B.A., and Harper, J.W. (2009). Ubiquitin-like protein activation by E1 enzymes: the apex for downstream signalling pathways. Nat. Rev. Mol. Cell Biol. *10*, 319–331. https://doi.org/10.1038/nrm2673.
16. Yuan, L., Lv, Z., Adams, M.J., and Olsen, S.K. (2021). Crystal structures of an E1-E2-ubiquitin thioester mimetic reveal molecular mechanisms of transthioesterification. Nat. Commun. *12*, 2370. https://doi.org/10.1038/s41467-021-22598-y.
17. Pruneda, J.N., Stoll, K.E., Bolton, L.J., Brzovic, P.S., and Klevit, R.E. (2011). Ubiquitin in motion: structural studies of the ubiquitin-conjugating enzyme approximately ubiquitin conjugate. Biochemistry *50*, 1624–1633. https://doi.org/10.1021/bi101913m.
18. Kochanczyk, T., Hann, Z.S., Lux, M.C., Delos Reyes, A.M.V., Ji, C., Tan, D.S., and Lima, C.D. (2024). Structural basis for transthiolation intermediates in the ubiquitin pathway. Nature *633*, 216–223. https://doi.org/10.1038/s41586-024-07828-9.
19. Dou, H., Buetow, L., Sibbet, G.J., Cameron, K., and Huang, D.T. (2012). BIRC7-E2 ubiquitin conjugate structure reveals the mechanism of ubiquitin transfer by a RING dimer. Nat. Struct. Mol. Biol. *19*, 876–883. https://doi.org/10.1038/nsmb.2379.
20. Metzger, M.B., Pruneda, J.N., Klevit, R.E., and Weissman, A.M. (2014). RING-type E3 ligases: master manipulators of E2 ubiquitin-conjugating enzymes and ubiquitination. Biochim. Biophys. Acta *1843*, 47–60. https://doi.org/10.1016/j.bbamcr.2013.05.026.
21. Komander, D., Clague, M.J., and Urbé, S. (2009). Breaking the chains: structure and function of the deubiquitinases. Nat. Rev. Mol. Cell Biol. *10*, 550–563. https://doi.org/10.1038/nrm2731.
22. Reyes-Turcu, F.E., Ventii, K.H., and Wilkinson, K.D. (2009). Regulation and cellular roles of ubiquitin-specific deubiquitinating enzymes. Annu. Rev. Biochem. *78*, 363–397. https://doi.org/10.1146/annurev.biochem.78.082307.091526.
23. Oh, E., Akopian, D., and Rape, M. (2018). Principles of Ubiquitin-Dependent Signaling. Annu. Rev. Cell Dev. Biol. *34*, 137–162. https://doi.org/10.1146/annurev-cellbio-100617-062802.

24. Deol, K.K., Lorenz, S., and Strieter, E.R. (2019). Enzymatic Logic of Ubiquitin Chain Assembly. Front. Physiol. *10*, 835. https://doi.org/10.3389/fphys.2019.00835.

25. Swatek, K.N., and Komander, D. (2016). Ubiquitin modifications. Cell Res. *26*, 399–422. https://doi.org/10.1038/cr.2016.39.

26. Nathan, J.A., Kim, H.T., Ting, L., Gygi, S.P., and Goldberg, A.L. (2013). Why do cellular proteins linked to K63-polyubiquitin chains not associate with proteasomes? EMBO J. *32*, 552–565. https://doi.org/10.1038/emboj.2012.354.

27. Liu, P., Gan, W., Su, S., Hauenstein, A.V., Fu, T.M., Brasher, B., Schwerdtfeger, C., Liang, A.C., Xu, M., and Wei, W. (2018). K63-linked polyubiquitin chains bind to DNA to facilitate DNA damage repair. Sci. Signal. *11*, eaar8133. https://doi.org/10.1126/scisignal.aar8133.

28. Abbott, D.W., Yang, Y., Hutti, J.E., Madhavarapu, S., Kelliher, M.A., and Cantley, L.C. (2007). Coordinated regulation of toll-like receptor and NOD2 signaling by k63-linked polyubiquitin chains. Mol. Cell Biol. *27*, 6012–6025. https://doi.org/10.1128/Mcb.00270-07.

29. Silva, G.M., Finley, D., and Vogel, C. (2015). K63 polyubiquitination is a new modulator of the oxidative stress response. Nat. Struct. Mol. Biol. *22*, 116–123. https://doi.org/10.1038/nsmb.2955.

30. Aguilar, R.C., and Wendland, B. (2003). Ubiquitin: not just for proteasomes anymore. Curr. Opin. Cell Biol. *15*, 184–190. https://doi.org/10.1016/s0955-0674(03)00010-3.

31. Hodge, C.D., Spyracopoulos, L., and Glover, J.N.M. (2016). Ubc13: the Lys63 ubiquitin chain building machine. Oncotarget *7*, 64471–64504. https://doi.org/10.18632/oncotarget.10948.

32. Jacobson, A.D., Zhang, N.Y., Xu, P., Han, K.J., Noone, S., Peng, J., and Liu, C.W. (2009). The lysine 48 and lysine 63 ubiquitin conjugates are processed differently by the 26 s proteasome. J. Biol. Chem. *284*, 35485–35494. https://doi.org/10.1074/jbc.M109.052928.

33. Duncan, L.M., Piper, S., Dodd, R.B., Saville, M.K., Sanderson, C.M., Luzio, J.P., and Lehner, P.J. (2006). Lysine-63-linked ubiquitination is required for endolysosomal degradation of class I molecules. EMBO J. *25*, 1635–1645. https://doi.org/10.1038/sj.emboj.7601056.

34. Ponts, N., Yang, J., Chung, D.W.D., Prudhomme, J., Girke, T., Horrocks, P., and Le Roch, K.G. (2008). Deciphering the Ubiquitin-Mediated Pathway in Apicomplexan Parasites: A Potential Strategy to Interfere with Parasite Virulence. PLoS One *3*, e2386. https://doi.org/10.1371/journal.pone.0002386.

35. Maneekesorn, S., Knuepfer, E., Green, J.L., Prommana, P., Uthaipibull, C., Srichairatanakool, S., and Holder, A.A. (2021). Deletion of Plasmodium falciparum ubc13 increases parasite sensitivity to the mutagen, methyl methanesulfonate and dihydroartemisinin. Sci. Rep. *11*, 21791. https://doi.org/10.1038/s41598-021-01267-6.

36. Wen, R., Wang, S., Xiang, D., Venglat, P., Shi, X., Zang, Y., Datla, R., Xiao, W., and Wang, H. (2014). UBC13, an E2 enzyme for Lys63-linked ubiquitination, functions in root development by affecting auxin signaling and Aux/IAA protein stability. Plant J. *80*, 424–436. https://doi.org/10.1111/tpj.12644.

37. Andersen, P.L., Zhou, H., Pastushok, L., Moraes, T., McKenna, S., Ziola, B., Ellison, M.J., Dixit, V.M., and Xiao, W. (2005). Distinct regulation of Ubc13 functions by the two ubiquitin-conjugating enzyme variants Mms2 and Uev1A. J. Cell Biol. *170*, 745–755. https://doi.org/10.1083/jcb.200502113.

38. Philip, N., and Haystead, T.A. (2007). Characterization of a UBC13 kinase in Plasmodium falciparum. Proc. Natl. Acad. Sci. USA *104*, 7845–7850. https://doi.org/10.1073/pnas.0611601104.

39. Raphemot, R., Eubanks, A.L., Toro-Moreno, M., Geiger, R.A., Hughes, P. F., Lu, K.Y., Haystead, T.A.J., and Derbyshire, E.R. (2019). Plasmodium PK9 Inhibitors Promote Growth of Liver-Stage Parasites. Cell Chem. Biol. *26*, 411–419.e7. https://doi.org/10.1016/j.chembiol.2018.11.003.

40. Narwal, S.K., Nayak, B., Mehra, P., and Mishra, S. (2022). Protein kinase 9 is not required for completion of the Plasmodium berghei life cycle. Microbiol. Res. *260*, 127051. https://doi.org/10.1016/j.micres.2022.127051.

41. Zhang, M., Wang, C., Otto, T.D., Oberstaller, J., Liao, X., Adapa, S.R., Udenze, K., Bronner, I.F., Casandra, D., Mayho, M., et al. (2018). Uncovering the essential genes of the human malaria parasite Plasmodium falciparum by saturation mutagenesis. Science *360*, eaap7847. https://doi.org/10.1126/science.aap7847.

42. Hodge, C.D., Edwards, R.A., Markin, C.J., McDonald, D., Pulvino, M., Huen, M.S.Y., Zhao, J., Spyracopoulos, L., Hendzel, M.J., and Glover, J.N.M. (2015). Covalent Inhibition of Ubc13 Affects Ubiquitin Signaling and Reveals Active Site Elements Important for Targeting. ACS Chem. Biol. *10*, 1718–1728. https://doi.org/10.1021/acschembio.5b00222.

43. Madeira, F., Pearce, M., Tivey, A.R.N., Basutkar, P., Lee, J., Edbali, O., Madhusoodanan, N., Kolesnikov, A., and Lopez, R. (2022). Search and sequence analysis tools services from EMBL-EBI in 2022. Nucleic Acids Res. *50*, W276–W279. https://doi.org/10.1093/nar/gkac240.

44. Pulvino, M., Liang, Y., Oleksyn, D., DeRan, M., Van Pelt, E., Shapiro, J., Sanz, I., Chen, L., and Zhao, J. (2012). Inhibition of proliferation and survival of diffuse large B-cell lymphoma cells by a small-molecule inhibitor of the ubiquitin-conjugating enzyme Ubc13-Uev1A. Blood *120*, 1668–1677. https://doi.org/10.1182/blood-2012-02-406074.

45. Cheng, J., Fan, Y.H., Xu, X., Zhang, H., Dou, J., Tang, Y., Zhong, X., Rojas, Y., Yu, Y., Zhao, Y., et al. (2014). A small-molecule inhibitor of UBE2N induces neuroblastoma cell death via activation of p53 and JNK pathways. Cell Death Dis. *5*, e1079. https://doi.org/10.1038/cddis.2014.54.

46. Gao, Y., Kwan, J., Orofino, J., Burrone, G., Mitra, S., Fan, T.Y., English, J., Hekman, R., Emili, A., Lyons, S.M., et al. (2024). Inhibition of K63 ubiquitination by G-Protein pathway suppressor 2 (GPS2) regulates mitochondria-associated translation. Pharmacol. Res. *207*, 107336. https://doi.org/10.1016/j.phrs.2024.107336.

47. Monda, J.K., and Cheeseman, I.M. (2018). Dynamic regulation of dynein localization revealed by small molecule inhibitors of ubiquitination enzymes. Open Biol. *8*, 180095. https://doi.org/10.1098/rsob.180095.

48. Pontrelli, P., Conserva, F., Papale, M., Oranger, A., Barozzino, M., Vocino, G., Rocchetti, M.T., Gigante, M., Castellano, G., Rossini, M., et al. (2017). Lysine 63 ubiquitination is involved in the progression of tubular damage in diabetic nephropathy. FASEB J. *31*, 308–319. https://doi.org/10.1096/fj.201600382RR.

49. Corteselli, E.M., Sharafi, M., Hondal, R., MacPherson, M., White, S., Lam, Y.W., Gold, C., Manuel, A.M., van der Vliet, A., Schneebeli, S.T., et al. (2023). Structural and functional fine mapping of cysteines in mammalian glutaredoxin reveal their differential oxidation susceptibility. Nat. Commun. *14*, 4550. https://doi.org/10.1038/s41467-023-39664-2.

50. Ramos-Guzman, C.A., Ruiz-Pernia, J.J., Zinovjev, K., and Tunon, I. (2023). Unveiling the Mechanistic Singularities of Caspases: A Computational Analysis of the Reaction Mechanism in Human Caspase-1. ACS Catal. *13*, 4348–4361. https://doi.org/10.1021/acscatal.3c00037.

51. Franklin, T.G., and Pruneda, J.N. (2019). A High-Throughput Assay for Monitoring Ubiquitination in Real Time. Front. Chem. *7*, 816. https://doi.org/10.3389/fchem.2019.00816.

52. Franklin, T.G., and Pruneda, J.N. (2023). Observing Real-Time Ubiquitination in High Throughput with Fluorescence Polarization. Methods Mol. Biol. *2581*, 3–12. https://doi.org/10.1007/978-1-0716-2784-6_1.

53. Kato, N., Comer, E., Sakata-Kato, T., Sharma, A., Sharma, M., Maetani, M., Bastien, J., Brancucci, N.M., Bittker, J.A., Corey, V., et al. (2016). Diversity-oriented synthesis yields novel multistage antimalarial inhibitors. Nature *538*, 344–349. https://doi.org/10.1038/nature19804.

54. Baniecki, M.L., Wirth, D.F., and Clardy, J. (2007). High-throughput Plasmodium falciparum growth assay for malaria drug discovery. Antimicrob. Agents Chemother. *51*, 716–723. https://doi.org/10.1128/AAC.01144-06.

55. McLean, K.J., Straimer, J., Hopp, C.S., Vega-Rodriguez, J., Small-Saunders, J.L., Kanatani, S., Tripathi, A., Mlambo, G., Dumoulin, P.C., Harris,

C.T., et al. (2019). Generation of Transmission-Competent Human Malaria Parasites with Chromosomally-Integrated Fluorescent Reporters. Sci. Rep. *9*, 13131. https://doi.org/10.1038/s41598-019-49348-x.

56. Vanheer, L.N., Zhang, H., Lin, G., and Kafsack, B.F.C. (2020). Activity of Epigenetic Inhibitors against Plasmodium falciparum Asexual and Sexual Blood Stages. Antimicrob. Agents Chemother. *64*, e02523-19. https://doi.org/10.1128/AAC.02523-19.

57. Derbyshire, E.R., Prudêncio, M., Mota, M.M., and Clardy, J. (2012). Liver-stage malaria parasites vulnerable to diverse chemical scaffolds. Proc. Natl. Acad. Sci. USA *109*, 8511–8516. https://doi.org/10.1073/pnas.1118370109.

58. Hjerpe, R., Aillet, F., Lopitz-Otsoa, F., Lang, V., England, P., and Rodriguez, M.S. (2009). Efficient protection and isolation of ubiquitylated proteins using tandem ubiquitin-binding entities. EMBO Rep. *10*, 1250–1258. https://doi.org/10.1038/embor.2009.192.

59. Kadimisetty, K., Sheets, K.J., Gross, P.H., Zerr, M.J., and Ouazia, D. (2021). Tandem Ubiquitin Binding Entities (TUBEs) as Tools to Explore Ubiquitin-Proteasome System and PROTAC Drug Discovery. Methods Mol. Biol. *2365*, 185–202. https://doi.org/10.1007/978-1-0716-1665-9_10.

60. Mata-Cantero, L., Azkargorta, M., Aillet, F., Xolalpa, W., LaFuente, M.J., Elortza, F., Carvalho, A.S., Martin-Plaza, J., Matthiesen, R., and Rodriguez, M.S. (2016). New insights into host-parasite ubiquitin proteome dynamics in infected red blood cells using a TUBEs-MS approach. J. Proteomics *139*, 45–59. https://doi.org/10.1016/j.jprot.2016.03.004.

61. Green, J.L., Wu, Y., Encheva, V., Lasonder, E., Prommaban, A., Kunzelmann, S., Christodoulou, E., Grainger, M., Truongvan, N., Bothe, S., et al. (2020). Ubiquitin activation is essential for schizont maturation in blood-stage development. PLoS Pathog. *16*, e1008640. https://doi.org/10.1371/journal.ppat.1008640.

62. Sheridan, C.M., Garcia, V.E., Ahyong, V., and DeRisi, J.L. (2018). The Plasmodium falciparum cytoplasmic translation apparatus: a promising therapeutic target not yet exploited by clinically approved anti-malarials. Malar. J. *17*, 465. https://doi.org/10.1186/s12936-018-2616-7.

63. Zhang, K., and Rathod, P.K. (2002). Divergent regulation of dihydrofolate reductase between malaria parasite and human host. Science *296*, 545–547. https://doi.org/10.1126/science.1068274.

64. Babai, R., Izrael, R., and Vértessy, B.G. (2022). Characterization of the dynamics of Plasmodium falciparum deoxynucleotide-triphosphate pool in a stage-specific manner. Sci. Rep. *12*, 19926. https://doi.org/10.1038/s41598-022-23807-4.

65. Hekmat-Nejad, M., and Rathod, P.K. (1997). Plasmodium falciparum: kinetic interactions of WR99210 with pyrimethamine-sensitive and pyrimethamine-resistant dihydrofolate reductase. Exp. Parasitol. *87*, 222–228. https://doi.org/10.1006/expr.1997.4228.

66. Xie, S.C., Wang, Y., Morton, C.J., Metcalfe, R.D., Dogovski, C., Pasaje, C.F.A., Dunn, E., Luth, M.R., Kumpornsin, K., Istvan, E.S., et al. (2024). Reaction hijacking inhibition of Plasmodium falciparum asparagine tRNA synthetase. Nat. Commun. *15*, 937. https://doi.org/10.1038/s41467-024-45224-z.

67. Xie, S.C., Metcalfe, R.D., Dunn, E., Morton, C.J., Huang, S.C., Puhalovich, T., Du, Y., Wittlin, S., Nie, S., Luth, M.R., et al. (2022). Reaction hijacking of tyrosine tRNA synthetase as a new whole-of-life-cycle antimalarial strategy. Science *376*, 1074–1079. https://doi.org/10.1126/science.abn0611.

68. Maxwell, B.A., Gwon, Y., Mishra, A., Peng, J., Nakamura, H., Zhang, K., Kim, H.J., and Taylor, J.P. (2021). Ubiquitination is essential for recovery of cellular activities after heat shock. Science *372*, eabc3593. https://doi.org/10.1126/science.abc3593.

69. Wu, B., Qiao, J., Wang, X., Liu, M., Xu, S., and Sun, D. (2021). Factors affecting the rapid changes of protein under short-term heat stress. BMC Genom. *22*, 263. https://doi.org/10.1186/s12864-021-07560-y.

70. Park, S., Lim, Y., Lee, D., Elvira, R., Lee, J.M., Lee, M.R., and Han, J. (2018). Modulation of Protein Synthesis by eIF2alpha Phosphorylation Protects Cell from Heat Stress-Mediated Apoptosis. Cells *7*, 254. https://doi.org/10.3390/cells7120254.

71. Cherkasov, V., Grousl, T., Theer, P., Vainshtein, Y., Glässer, C., Mongis, C., Kramer, G., Stoecklin, G., Knop, M., Mogk, A., and Bukau, B. (2015). Systemic control of protein synthesis through sequestration of translation and ribosome biogenesis factors during severe heat stress. FEBS Lett. *589*, 3654–3664. https://doi.org/10.1016/j.febslet.2015.10.010.

72. Yang, T., Yeoh, L.M., Tutor, M.V., Dixon, M.W., McMillan, P.J., Xie, S.C., Bridgford, J.L., Gillett, D.L., Duffy, M.F., Ralph, S.A., et al. (2019). Decreased K13 Abundance Reduces Hemoglobin Catabolism and Proteotoxic Stress, Underpinning Artemisinin Resistance. Cell Rep. *29*, 2917–2928.e5. https://doi.org/10.1016/j.celrep.2019.10.095.

73. Chung, D.W.D., and Le Roch, K.G. (2010). Targeting the Plasmodium ubiquitin/proteasome system with anti-malarial compounds: promises for the future. Infect. Disord.: Drug Targets *10*, 158–164. https://doi.org/10.2174/187152610791163345.

74. Le Roch, K.G., Johnson, J.R., Florens, L., Zhou, Y., Santrosyan, A., Grainger, M., Yan, S.F., Williamson, K.C., Holder, A.A., Carucci, D.J., et al. (2004). Global analysis of transcript and protein levels across the Plasmodium falciparum life cycle. Genome Res. *14*, 2308–2318. https://doi.org/10.1101/gr.2523904.

75. Siddiqui, G., De Paoli, A., MacRaild, C.A., Sexton, A.E., Boulet, C., Shah, A.D., Batty, M.B., Schittenhelm, R.B., Carvalho, T.G., and Creek, D.J. (2022). A new mass spectral library for high-coverage and reproducible analysis of the Plasmodium falciparum-infected red blood cell proteome. GigaScience *11*, giac008. https://doi.org/10.1093/gigascience/giac008.

76. Tarun, A.S., Peng, X., Dumpit, R.F., Ogata, Y., Silva-Rivera, H., Camargo, N., Daly, T.M., Bergman, L.W., and Kappe, S.H.I. (2008). A combined transcriptome and proteome survey of malaria parasite liver stages. Proc. Natl. Acad. Sci. USA *105*, 305–310. https://doi.org/10.1073/pnas.0710780104.

77. Fukushima, T., Matsuzawa, S.i., Kress, C.L., Bruey, J.M., Krajewska, M., Lefebvre, S., Zapata, J.M., Ronai, Z., and Reed, J.C. (2007). Ubiquitin-conjugating enzyme Ubc13 is a critical component of TNF receptor-associated factor (TRAF)-mediated inflammatory responses. Proc. Natl. Acad. Sci. USA *104*, 6371–6376. https://doi.org/10.1073/pnas.0700548104.

78. Yamamoto, M., Sato, S., Saitoh, T., Sakurai, H., Uematsu, S., Kawai, T., Ishii, K.J., Takeuchi, O., and Akira, S. (2006). Cutting Edge: Pivotal function of Ubc13 in thymocyte TCR signaling. J. Immunol. *177*, 7520–7524. https://doi.org/10.4049/jimmunol.177.11.7520.

79. Huang, F., Han, X., Xiao, X., and Zhou, J. (2022). Covalent Warheads Targeting Cysteine Residue: The Promising Approach in Drug Development. Molecules *27*, 7728. https://doi.org/10.3390/molecules27227728.

80. Resnick, E., Bradley, A., Gan, J., Douangamath, A., Krojer, T., Sethi, R., Geurink, P.P., Aimon, A., Amitai, G., Bellini, D., et al. (2019). Rapid Covalent-Probe Discovery by Electrophile-Fragment Screening. J. Am. Chem. Soc. *141*, 8951–8968. https://doi.org/10.1021/jacs.9b02822.

81. Kuljanin, M., Mitchell, D.C., Schweppe, D.K., Gikandi, A.S., Nusinow, D.P., Bulloch, N.J., Vinogradova, E.V., Wilson, D.L., Kool, E.T., Mancias, J.D., et al. (2021). Reimagining high-throughput profiling of reactive cysteines for cell-based screening of large electrophile libraries. Nat. Biotechnol. *39*, 630–641. https://doi.org/10.1038/s41587-020-00778-3.

82. Imhoff, R.D., Rosenthal, M.R., Ashraf, K., Bhanot, P., Ng, C.L., and Flaherty, D.P. (2023). Identification of covalent fragment inhibitors for Plasmodium falciparum UCHL3 with anti-malarial efficacy. Bioorg. Med. Chem. Lett. *94*, 129458. https://doi.org/10.1016/j.bmcl.2023.129458.

83. Riley, N.M., and Coon, J.J. (2016). Phosphoproteomics in the Age of Rapid and Deep Proteome Profiling. Anal. Chem. *88*, 74–94. https://doi.org/10.1021/acs.analchem.5b04123.

84. Macek, B., Mann, M., and Olsen, J.V. (2009). Global and site-specific quantitative phosphoproteomics: principles and applications. Annu.

Rev. Pharmacol. Toxicol. *49*, 199–221. https://doi.org/10.1146/annurev.pharmtox.011008.145606.

85. Alam, M.M., Solyakov, L., Bottrill, A.R., Flueck, C., Siddiqui, F.A., Singh, S., Mistry, S., Viskaduraki, M., Lee, K., Hopp, C.S., et al. (2015). Phosphoproteomics reveals malaria parasite Protein Kinase G as a signalling hub regulating egress and invasion. Nat. Commun. *6*, 7285. https://doi.org/10.1038/ncomms8285.

86. Solyakov, L., Halbert, J., Alam, M.M., Semblat, J.P., Dorin-Semblat, D., Reininger, L., Bottrill, A.R., Mistry, S., Abdi, A., Fennell, C., et al. (2011). Global kinomic and phospho-proteomic analyses of the human malaria parasite Plasmodium falciparum. Nat. Commun. *2*, 565. https://doi.org/10.1038/ncomms1558.

87. Pease, B.N., Huttlin, E.L., Jedrychowski, M.P., Dorin-Semblat, D., Sebastiani, D., Segarra, D.T., Roberts, B.F., Chakrabarti, R., Doerig, C., Gygi, S.P., and Chakrabarti, D. (2018). Characterization of Plasmodium falciparum Atypical Kinase PfPK7(-) Dependent Phosphoproteome. J. Proteome Res. *17*, 2112–2123. https://doi.org/10.1021/acs.jproteome.8b00062.

88. Tsai, C.F., Ogata, K., Sugiyama, N., and Ishihama, Y. (2022). Motif-centric phosphoproteomics to target kinase-mediated signaling pathways. Cell Rep. Methods *2*, 100138. https://doi.org/10.1016/j.crmeth.2021.100138.

89. Ong, H.W., de Silva, C., Avalani, K., Kwarcinski, F., Mansfield, C.R., Chirgwin, M., Truong, A., Derbyshire, E.R., Zutshi, R., and Drewry, D.H. (2023). Characterization of 2,4-Dianilinopyrimidines Against Five Kinases PfARK1, PfARK3, PfNEK3, PfPK9, and PfPKB. ACS Med. Chem. Lett. *14*, 1774–1784. https://doi.org/10.1021/acsmedchemlett.3c00354.

90. Arora, P., Narwal, M., Thakur, V., Mukhtar, O., Malhotra, P., and Mohmmed, A. (2023). A Plasmodium falciparum ubiquitin-specific protease (PfUSP) is essential for parasite survival and its disruption enhances artemisinin efficacy. Biochem. J. *480*, 25–39. https://doi.org/10.1042/BCJ20220429.

91. Simwela, N.V., Hughes, K.R., Rennie, M.T., Barrett, M.P., and Waters, A.P. (2021). Mammalian Deubiquitinating Enzyme Inhibitors Display in Vitro and in Vivo Activity against Malaria Parasites and Potentiate Artemisinin Action. ACS Infect. Dis. *7*, 333–346. https://doi.org/10.1021/acsinfecdis.0c00580.

92. Wang, L., Delahunty, C., Fritz-Wolf, K., Rahlfs, S., Helena Prieto, J., Yates, J.R., and Becker, K. (2015). Characterization of the 26S proteasome network in Plasmodium falciparum. Sci. Rep. *5*, 17818. https://doi.org/10.1038/srep17818.

93. Wilde, M.L., Ruparel, U., Klemm, T., Lee, V.V., Calleja, D.J., Komander, D., and Tonkin, C.J. (2023). Characterisation of the OTU domain deubiquitinase complement of Toxoplasma gondii. Life Sci. Alliance *6*, e202201710. https://doi.org/10.26508/lsa.202201710.

94. Yates, J.R., Ruse, C.I., and Nakorchevsky, A. (2009). Proteomics by mass spectrometry: approaches, advances, and applications. Annu. Rev. Biomed. Eng. *11*, 49–79. https://doi.org/10.1146/annurev-bioeng-061008-124934.

95. Bantscheff, M., Lemeer, S., Savitski, M.M., and Kuster, B. (2012). Quantitative mass spectrometry in proteomics: critical review update from 2007 to the present. Anal. Bioanal. Chem. *404*, 939–965. https://doi.org/10.1007/s00216-012-6203-4.

96. Back, S., Gorman, A.W., Vogel, C., and Silva, G.M. (2019). Site-Specific K63 Ubiquitinomics Provides Insights into Translation Regulation under Stress. J. Proteome Res. *18*, 309–318. https://doi.org/10.1021/acs.jproteome.8b00623.

97. Li, Z., Cheng, Z., Raghothama, C., Cui, Z., Liu, K., Li, X., Jiang, C., Jiang, W., Tan, M., Ni, X., et al. (2018). USP9X controls translation efficiency via deubiquitination of eukaryotic translation initiation factor 4A1. Nucleic Acids Res. *46*, 823–839. https://doi.org/10.1093/nar/gkx1226.

98. Murata, T., and Shimotohno, K. (2006). Ubiquitination and proteasome-dependent degradation of human eukaryotic translation initiation factor 4E. J. Biol. Chem. *281*, 20788–20800. https://doi.org/10.1074/jbc.M600563200.

99. Tuckow, A.P., Kazi, A.A., Kimball, S.R., and Jefferson, L.S. (2013). Identification of ubiquitin-modified lysine residues and novel phosphorylation sites on eukaryotic initiation factor 2B epsilon. Biochem. Biophys. Res. Commun. *436*, 41–46. https://doi.org/10.1016/j.bbrc.2013.05.053.

100. Zong, N., Ping, P., Lau, E., Choi, H.J., Ng, D.C., Meyer, D., Fang, C., Li, H., Wang, D., Zelaya, I.M., et al. (2014). Lysine ubiquitination and acetylation of human cardiac 20S proteasomes. Proteomics. Clin. Appl. *8*, 590–594. https://doi.org/10.1002/prca.201400029.

101. Tsimokha, A.S., Artamonova, T.O., Diakonov, E.E., Khodorkovskii, M.A., and Tomilin, A.N. (2020). Post-Translational Modifications of Extracellular Proteasome. Molecules *25*, 3504. https://doi.org/10.3390/molecules25153504.

102. Besche, H.C., Sha, Z., Kukushkin, N.V., Peth, A., Hock, E.M., Kim, W., Gygi, S., Gutierrez, J.A., Liao, H., Dick, L., and Goldberg, A.L. (2014). Autoubiquitination of the 26S proteasome on Rpn13 regulates breakdown of ubiquitin conjugates. EMBO J. *33*, 1159–1176. https://doi.org/10.1002/embj.201386906.

103. Kors, S., Geijtenbeek, K., Reits, E., and Schipper-Krom, S. (2019). Regulation of Proteasome Activity by (Post-)transcriptional Mechanisms. Front. Mol. Biosci. *6*, 48. https://doi.org/10.3389/fmolb.2019.00048.

104. Romero-Barrios, N., and Vert, G. (2018). Proteasome-independent functions of lysine-63 polyubiquitination in plants. New Phytol. *217*, 995–1011. https://doi.org/10.1111/nph.14915.

105. Tan, J.M.M., Wong, E.S.P., Kirkpatrick, D.S., Pletnikova, O., Ko, H.S., Tay, S.P., Ho, M.W.L., Troncoso, J., Gygi, S.P., Lee, M.K., et al. (2008). Lysine 63-linked ubiquitination promotes the formation and autophagic clearance of protein inclusions associated with neurodegenerative diseases. Hum. Mol. Genet. *17*, 431–439. https://doi.org/10.1093/hmg/ddm320.

106. Saeed, B., Deligne, F., Brillada, C., Dünser, K., Ditengou, F.A., Turek, I., Allahham, A., Grujic, N., Dagdas, Y., Ott, T., et al. (2023). K63-linked ubiquitin chains are a global signal for endocytosis and contribute to selective autophagy in plants. Curr. Biol. *33*, 1337–1345.e5. https://doi.org/10.1016/j.cub.2023.02.024.

107. Clough, B., Wright, J.D., Pereira, P.M., Hirst, E.M., Johnston, A.C., Henriques, R., and Frickel, E.M. (2016). K63-Linked Ubiquitination Targets Toxoplasma gondii for Endo-lysosomal Destruction in IFNgamma-Stimulated Human Cells. PLoS Pathog. *12*, e1006027. https://doi.org/10.1371/journal.ppat.1006027.

108. Forte, N., Dovala, D., Hesse, M.J., McKenna, J.M., Tallarico, J.A., Schirle, M., and Nomura, D.K. (2023). Targeted Protein Degradation through E2 Recruitment. ACS Chem. Biol. *18*, 897–904. https://doi.org/10.1021/acschembio.3c00040.

109. Paudel, R.R., Lu, D., Roy Chowdhury, S., Monroy, E.Y., and Wang, J. (2023). Targeted Protein Degradation via Lysosomes. Biochemistry *62*, 564–579. https://doi.org/10.1021/acs.biochem.2c00310.

110. Halim, V.A., García-Santisteban, I., Warmerdam, D.O., van den Broek, B., Heck, A.J.R., Mohammed, S., and Medema, R.H. (2018). Doxorubicin-induced DNA Damage Causes Extensive Ubiquitination of Ribosomal Proteins Associated with a Decrease in Protein Translation. Mol. Cell. Proteomics *17*, 2297–2308. https://doi.org/10.1074/mcp.RA118.000652.

111. Boon, N.J., Oliveira, R.A., Körner, P.R., Kochavi, A., Mertens, S., Malka, Y., Voogd, R., van der Horst, S.E.M., Huismans, M.A., Smabers, L.P., et al. (2024). DNA damage induces p53-independent apoptosis through ribosome stalling. Science *384*, 785–792. https://doi.org/10.1126/science.adh7950.

112. Goyal, M., Heinberg, A., Mitesser, V., Kandelis-Shalev, S., Singh, B.K., and Dzikowski, R. (2021). Phosphorylation of the Canonical Histone H2A Marks Foci of Damaged DNA in Malaria Parasites. mSphere *6*, e01131-20. https://doi.org/10.1128/mSphere.01131-20.

113. Badugu, S.B., Nabi, S.A., Vaidyam, P., Laskar, S., Bhattacharyya, S., and Bhattacharyya, M.K. (2015). Identification of Plasmodium falciparum DNA Repair Protein Mre11 with an Evolutionarily Conserved Nuclease Function. PLoS One *10*, e0125358. https://doi.org/10.1371/journal.pone.0125358.

114. Gershon, P.D., and Howells, R.E. (1986). Mitochondrial protein synthesis in Plasmodium falciparum. Mol. Biochem. Parasitol. *18*, 37–43. https://doi.org/10.1016/0166-6851(86)90048-4.

115. Ke, H., Dass, S., Morrisey, J.M., Mather, M.W., and Vaidya, A.B. (2018). The mitochondrial ribosomal protein L13 is critical for the structural and functional integrity of the mitochondrion in Plasmodium falciparum. J. Biol. Chem. *293*, 8128–8137. https://doi.org/10.1074/jbc.RA118.002552.

116. Dass, S., Mather, M.W., Morrisey, J.M., Ling, L., Vaidya, A.B., and Ke, H. (2022). Transcriptional changes in Plasmodium falciparum upon conditional knock down of mitochondrial ribosomal proteins RSM22 and L23. PLoS One *17*, e0274993. https://doi.org/10.1371/journal.pone.0274993.

117. Vringer, E., Heilig, R., Riley, J.S., Black, A., Cloix, C., Skalka, G., Montes-Gómez, A.E., Aguado, A., Lilla, S., Walczak, H., et al. (2024). Mitochondrial outer membrane integrity regulates a ubiquitin-dependent and NF-kappaB-mediated inflammatory response. EMBO J. *43*, 904–930. https://doi.org/10.1038/s44318-024-00044-1.

118. Singh, A., Tiwari, S., and Singh, S. (2024). Pirh2 modulates the mitochondrial function and cytochrome c-mediated neuronal death during Alzheimer's disease. Cell Death Dis. *15*, 331. https://doi.org/10.1038/s41419-024-06662-1.

119. Prajapati, S.K., Ayanful-Torgby, R., Pava, Z., Barbeau, M.C., Acquah, F. K., Cudjoe, E., Kakaney, C., Amponsah, J.A., Obboh, E., Ahmed, A.E., et al. (2020). The transcriptome of circulating sexually committed Plasmodium falciparum ring stage parasites forecasts malaria transmission potential. Nat. Commun. *11*, 6159. https://doi.org/10.1038/s41467-020-19988-z.

120. Cheramangalam, R.N., Anand, T., Pandey, P., Balasubramanian, D., Varghese, R., Singhal, N., Jaiswal, S.N., and Jaiswal, M. (2023). Bendless is essential for PINK1-Park mediated Mitofusin degradation under mitochondrial stress caused by loss of LRPPRC. PLoS Genet. *19*, e1010493. https://doi.org/10.1371/journal.pgen.1010493.

121. Sakata-Kato, T., and Wirth, D.F. (2016). A Novel Methodology for Bioenergetic Analysis of Plasmodium falciparum Reveals a Glucose-Regulated Metabolic Shift and Enables Mode of Action Analyses of Mitochondrial Inhibitors. ACS Infect. Dis. *2*, 903–916. https://doi.org/10.1021/acsinfecdis.6b00101.

122. Ramesh, S., Cihalova, D., Rajendran, E., Van Dooren, G.G., and Maier, A. G. (2023). Analysis of Plasmodium falciparum Mitochondrial Electron Transport Chain Activity Using Seahorse XFe96 Extracellular Flux Assays. Bio. Protoc. *13*, e4863. https://doi.org/10.21769/BioProtoc.4863.

123. Kumari, V., Vidyarthi, S., Tripathi, A., Chaurasia, N., Rai, N., Shukla, R., Noorie, S.N., Bhati, G., Anjum, S., Anas, M., et al. (2025). Understanding the Role of RING-Between-RING E3 Ligase of the Human Malaria Parasite. Proteins. https://doi.org/10.1002/prot.26813.

124. Mansson, R., Tsapogas, P., Akerlund, M., Lagergren, A., Gisler, R., and Sigvardsson, M. (2004). Pearson correlation analysis of microarray data allows for the identification of genetic targets for early B-cell factor. J. Biol. Chem. *279*, 17905–17913. https://doi.org/10.1074/jbc.M400589200.

125. Bhardwaj, N., and Lu, H. (2005). Correlation between gene expression profiles and protein-protein interactions within and across genomes. Bioinformatics *21*, 2730–2738. https://doi.org/10.1093/bioinformatics/bti398.

126. Borrmann, S., Straimer, J., Mwai, L., Abdi, A., Rippert, A., Okombo, J., Muriithi, S., Sasi, P., Kortok, M.M., Lowe, B., et al. (2013). Genome-wide screen identifies new candidate genes associated with artemisinin susceptibility in Plasmodium falciparum in Kenya. Sci. Rep. *3*, 3318. https://doi.org/10.1038/srep03318.

127. Smith, C., Hajisadeghian, M., van Noort, G., Deery, M.J., Pinto-Fernandez, A., Kessler, B.M., and Artavanis-Tsakonas, K. (2025). Activity-based protein profiling reveals both canonical and novel ubiquitin pathway enzymes in plasmodium. PLoS Pathog. *21*, e1013032. https://doi.org/10.1371/journal.ppat.1013032.

128. Sommer, S., Ritterhoff, T., Melchior, F., and Mootz, H.D. (2015). A stable chemical SUMO1-Ubc9 conjugate specifically binds as a thioester mimic to the RanBP2-E3 ligase complex. Chembiochem *16*, 1183–1189. https://doi.org/10.1002/cbic.201500011.

129. Xu, L., Fan, J., Wang, Y., Zhang, Z., Fu, Y., Li, Y.M., and Shi, J. (2019). An activity-based probe developed by a sequential dehydroalanine formation strategy targets HECT E3 ubiquitin ligases. Chem. Commun. *55*, 7109–7112. https://doi.org/10.1039/c9cc03739j.

130. Mathur, S., Fletcher, A.J., Branigan, E., Hay, R.T., and Virdee, S. (2020). Photocrosslinking Activity-Based Probes for Ubiquitin RING E3 Ligases. Cell Chem. Biol. *27*, 74–82.e6. https://doi.org/10.1016/j.chembiol.2019.11.013.

131. Pao, K.C., Wood, N.T., Knebel, A., Rafie, K., Stanley, M., Mabbitt, P.D., Sundaramoorthy, R., Hofmann, K., van Aalten, D.M.F., and Virdee, S. (2018). Activity-based E3 ligase profiling uncovers an E3 ligase with esterification activity. Nature *556*, 381–385. https://doi.org/10.1038/s41586-018-0026-1.

132. Mulder, M.P.C., Witting, K., Berlin, I., Pruneda, J.N., Wu, K.P., Chang, J. G., Merkx, R., Bialas, J., Groettrup, M., Vertegaal, A.C.O., et al. (2016). A cascading activity-based probe sequentially targets E1-E2-E3 ubiquitin enzymes. Nat. Chem. Biol. *12*, 523–530. https://doi.org/10.1038/nchembio.2084.

133. Zhao, B., Tsai, Y.C., Jin, B., Wang, B., Wang, Y., Zhou, H., Carpenter, T., Weissman, A.M., and Yin, J. (2020). Protein Engineering in the Ubiquitin System: Tools for Discovery and Beyond. Pharmacol. Rev. *72*, 380–413. https://doi.org/10.1124/pr.118.015651.

134. van Tilburg, G.B., Elhebieshy, A.F., and Ovaa, H. (2016). Synthetic and semi-synthetic strategies to study ubiquitin signaling. Curr. Opin. Struct. Biol. *38*, 92–101. https://doi.org/10.1016/j.sbi.2016.05.022.

135. Shannon, P., Markiel, A., Ozier, O., Baliga, N.S., Wang, J.T., Ramage, D., Amin, N., Schwikowski, B., and Ideker, T. (2003). Cytoscape: a software environment for integrated models of biomolecular interaction networks. Genome Res. *13*, 2498–2504. https://doi.org/10.1101/gr.1239303.

136. Supek, F., Bošnjak, M., Škunca, N., and Šmuc, T. (2011). REVIGO summarizes and visualizes long lists of gene ontology terms. PLoS One *6*, e21800. https://doi.org/10.1371/journal.pone.0021800.

137. Mansfield, C.R., Quan, B., Chirgwin, M.E., Eduful, B., Hughes, P.F., Neveu, G., Sylvester, K., Ryan, D.H., Kafsack, B.F.C., Haystead, T.A.J., et al. (2024). Selective targeting of Plasmodium falciparum Hsp90 disrupts the 26S proteasome. Cell Chem. Biol. *31*, 729–742.e13. https://doi.org/10.1016/j.chembiol.2024.02.008.

138. Fivelman, Q.L., McRobert, L., Sharp, S., Taylor, C.J., Saeed, M., Swales, C.A., Sutherland, C.J., and Baker, D.A. (2007). Improved synchronous production of Plasmodium falciparum gametocytes in vitro. Mol. Biochem. Parasitol. *154*, 119–123. https://doi.org/10.1016/j.molbiopara.2007.04.008.

139. McDowell, G.S., Gaun, A., and Steen, H. (2013). iFASP: combining isobaric mass tagging with filter-aided sample preparation. J. Proteome Res. *12*, 3809–3812. https://doi.org/10.1021/pr400032m.

STAR★METHODS

KEY RESOURCES TABLE

REAGENT or RESOURCE	SOURCE	IDENTIFIER
Antibodies		
Rabbit monoclonal anti-ubiquitin (linkage-specific K63)	Abcam	Cat# ab179434; RRID: AB_2895239
Rabbit monoclonal anti-ubiquitin (linkage-specific K48)	Abcam	Cat# ab140601; RRID: AB_2783797
Rabbit polyclonal anti-ubiquitin	Abcam	Cat# ab7780; RRID: AB_306069
Goat polyclonal anti-UIS4	Antibodies.com	Cat# A121573
HisProbe™-HRP Conjugate	Thermo Fisher Scientific	Cat# 15165
Bacterial and virus strains		
E. coli BL21(DE3)	New England Biolabs	Cat# C2527
E. coli NEB5α	New England Biolabs	Cat# C2987
Biological samples		
Human Blood	Gulf Coast Regional Blood Center	N/A
P. berghei ANKA infected *Anopheles stephensi* mosquitoes	University of Georgia SporoCore	N/A
Chemicals, peptides, and recombinant proteins		
HisPur™ Ni-NTA Resin	Thermo Fisher Scientific	Cat# 88221
GST Sepharose® 4B resin	Sigma-Aldrich	Cat# GE17-0756-01
cOmplete Ultra EDTA-free	Sigma-Aldrich	Cat# 5892953001
SYBR™ Green I	Invitrogen	Cat# S7563
K63-TUBE (magnetic beads)	LifeSensors	Cat# UM-0404M-1000
Control magnetic beads (negative control)	LifeSensors	Cat# UM-0400M-1000
NSC697923	Selleck Chemicals	Cat# S7142
Bruceantin	MedChemExpress	Cat# HY-N0840
WR99210 hydrochloride	Sigma-Aldrich	Cat# SML2976
Alpha-dihydroartemisinin	Beantown Chemical	Cat# 123740-1G
Chloroquine diphosphate salt	Sigma-Aldrich	Cat# C6628
O-propargyl-puromycin	Vector Laboratories	Cat# CCT-1407
Azide-flour 488	Sigma-Aldrich	Cat# 760765
Ubiquitin	R&D Systems	Cat# U-530
Fluorescein-ubiquitin	R&D Systems	Cat# U-590
HsUBA1	Sino Biological	Cat# 103612-944
PfUBA1-His6	This paper	N/A
HsUbc13	This paper	N/A
PfUbc13-His6	This paper	N/A
PfUbc13^{C86S}-His6	This paper	N/A
PreScission Protease	Cytiva	Cat# 27084301
Critical commercial assays		
Pierce™ Coomassie Plus Bradford Assay	Thermo Fisher Scientific	Cat# 23236
Bright-Glo™ Luciferase Assay System	Promega	Cat# G6081
CellTiter-Fluor™ Cell Viability Assay	Promega	Cat# E2620
Hemacolor© Stain Set	Sigma-Aldrich	Cat# 65044-93
Q5© Site-Directed Mutagenesis Kit	New England Biolabs	Cat# E0554S
Deposited data		
K63-TUBEs bottom-up proteomics raw data	This paper	ProteomeXchange: PXD059643

(*Continued on next page*)

Continued

REAGENT or RESOURCE	SOURCE	IDENTIFIER
Experimental models: Cell lines		
Human: HepG2 cells	Duke Cell Culture Facility	N/A
Experimental models: Organisms/strains		
P. falciparum 3D7	BEI Resources Repository; contributed by Daniel J. Carucci	MRA-102
P. falciparum Dd2	BEI Resources Repository; contributed by Thomas E. Wellems	MRA-156
P. falciparum Dd2-R539T	BEI Resources Repository; contributed by David A. Fidock	MRA-1255
P. falciparum W2	BEI Resources Repository; contributed by Dennis E. Kyle	MRA-157
P. falciparum NF54 peg4-tdTomato	Laboratory of Photini Sinnis	N/A
P. berghei-Luc ANKA	University of Georgia SporoCore	N/A
Oligonucleotides		
Primer: PfUbc13 (C86S) mutagenesis Forward: GGTCGAATTTCCTTAGA TATATTAAAAGATAAATG	This paper	N/A
Primer: PfUbc13 (C86S) mutagenesis Reverse: TAACTTATCAATATTTGGA TGATATATTTTTG	This paper	N/A
Recombinant DNA		
PfUBA1-His6 (pET-28a)	This paper	Twist Bioscience
HsUbc13-GST (pGEX6)	Gift from Dr. Wei Xiao (University of Saskatchewan)	N/A
PfUbc13-His6 (pET-21a)	Raphemot et al.[39]	N/A
PfUbc13^{C86S}-His6 (pET-21a)	This paper	N/A
Software and algorithms		
ChemDraw Professional 23.1	PerkinElmer	https://www.perkinelmer.com/category/chemdraw
GraphPad Prism 10	GraphPad software	https://www.graphpad.com/
Schrödinger Release 2024-4: Maestro	Schrödinger, LLC	https://www.schrodinger.com/products/maestro
Clustal Omega	Madeira et al.[43]	https://www.ebi.ac.uk/Tools/msa/clustalo/
Cytoscape 3.10.3	Shannon et al.[135]	https://cytoscape.org
PlasmoDB	The *Plasmodium* Genome Database Collaborative	https://plasmodb.org/plasmo/app/
REVIGO	Supek at al.[136]	http://revigo.irb.hr/
ImageJ	NIH	https://imagej.nih.gov/ij/
Other		
Non-treated black 96 well plates	Corning	Cat# 3915
Non-binding black 384 well plates	Corning	Cat# 3575
Tissue culture treated white 384 well plates	Corning	Cat# 3570

EXPERIMENTAL MODEL AND STUDY PARTICIPANT DETAILS

Cell lines

HepG2 cells were obtained through the Duke Cell Culture Facility. Independent cell line authentication was not conducted after purchase. Cell morphology was regularly assessed by microscopy, and no commonly misidentified cell lines are cultured in lab. Cell lines were routinely tested for mycoplasma contamination. The sex of the cell line is male. Cells were cultured in Dulbecco's Modified Eagle Medium (DMEM) with L-glutamine (Gibco) supplemented with 10% heat-inactivated fetal bovine serum (HI-FBS) (v/v) (Sigma-Aldrich) and 1% antibiotic-antimycotic (Thermo Fisher Scientific) at 37°C with 5% CO_2.

Parasite lines

P. falciparum 3D7, Dd2, Dd2-R539T, and W2 were obtained from BEI Resources, NIAID, NIH, (MRA-102, MRA-156, MRA-1255, MRA-157, respectively). *P. falciparum* NF54 peg4-tdTomato were obtained from the laboratory of Photini Sinnis. Blood stage *P. falciparum* were grown in 10.44 g/L RPMI 1640 (Gibco), 25 mM HEPES, pH 7.2, 0.37 mM hypoxanthine, 24 mM sodium bicarbonate, 0.5% (wt/vol) AlbuMAX II (Gibco), and 25 mg/mL gentamicin. Cultures were maintained at 37°C with 3% O_2, 5%CO_2, and 92% N_2. Whole blood samples were obtained from Gulf Coast Regional Blood Center, and fresh erythrocytes were added to cultures for blood stage *P. falciparum* invasion. For liver stage cultures, *P. berghei* ANKA infected *Anopheles stephensi* mosquitoes were purchased from the University of Georgia SporoCore.

Bacterial strains

E. coli NEB5α (NEB) and BL21(DE3) (NEB) were used for plasmid and protein expression, respectively. Bacteria were propagated on Difco™ Luria-Bertani (Miller) agar plates and cultured in Difco™ Luria-Bertani (Miller) broth.

METHOD DETAILS

Molecular modeling

Ligand docking was performed using Schrödinger Maestro, release 2024-4 (Schrödinger, LLC: New York, NY, 2024). NSC697923 was downloaded as a .sdf file from ChemDraw and processed using the LigPrep module with default parameters. Solved or predicted protein structures were downloaded as .pdb files from either the RCSB Protein Data Bank (https://www.rcsb.org) or AlphaFold (https://alphafold.ebi.ac.uk), respectively. The downloaded protein structures were prepared using the Protein Preparation Workflow module with default parameters. All unnecessary chains and molecules were removed. The grid boxes (15 × 15 Angstrom) were generated using the Receptor Grid Generation module with the centroid defined as the predicted catalytic cysteine. Docking was performed using XP-Glide in the Ligand Docking module with default settings. A maximum of 10 poses were generated with post-docking minimization, and the results were manually reviewed and selected. MM/GBSA values were calculated using the Prime-MM/GBSA module with default parameters. Structural alignments were performed using the Superposition tool with default parameters, and C-alpha RMSD values were calculated with HsUbc13 (PDB 9BIV) as the reference structure.

Protein expression and purification

Plasmids (pET-21a_PfUbc13,[39] pGEx6_HsUbc13,[39] and pET-28a_PfUBA1 (Twist Biosciences, codon-optimized)) were transformed into *E. coli* BL21(DE3) cells (New England Biolabs). Plasmid pET-21a_PfUbc13^{C86S} was generated using site-directed mutagenesis (Q5 site-directed mutagenesis kit) per the manufacturer's protocol (New England Biolabs) using primers purchased from Eton. All plasmid constructs were confirmed by sequencing (Eton). For protein expression, *E. coli* was grown at 37°C, 250 rpm in 1 L of Luria-Bertani broth with ampicillin (100 μg/mL) or kanamycin (50 μg/mL) until the optical density at 600 nm reached 0.6. Protein expression was then induced with 100 μM isopropyl β-D-1-thiogalactopyranoside (IPTG), and cells were grown for 16-18 hours at 18°C, 250 rpm. Cells were collected by centrifugation at 4,300 g and stored at −80°C until purification.

For His-tagged proteins (pET-21a_PfUbc13, pET-21a_PfUbc13^{C86S}, pET-28a_PfUBA1), cells were resuspended in lysis buffer (50 mM KH_2PO_4, pH 8.0, 200 mM NaCl, 5% glycerol, 1 mM imidazole, 1 mM benzamidine, 5 mM β-mercaptoethanol, 1 cOmplete protease inhibitor tablet (Roche)) and lysed via sonication using a FB120 Sonic Dismembrator (Fisher Scientific). Lysate was centrifuged at 4,300 g for 3-4 hours and then incubated with Ni-nitrilotriacetic acid agarose (Qiagen) overnight at 4°C with rotation. The protein-bound resin was washed with buffer (50 mM KH_2PO_4, pH 8.0, 200 mM NaCl, 5% glycerol, 5 mM β-mercaptoethanol, 1 mM imidazole), and protein was eluted with increasing concentrations of imidazole (1–150 mM) using a BioLogic low pressure chromatography system (Bio-Rad).

For GST-tagged proteins (PGEX6_HsUbc13), cells were resuspended in GST buffer (50 mM Tris-HCl, pH 7.5, 150 mM NaCl, 1 mM DTT, 5% glycerol, 5 mM EDTA, 1 mM benzamidine). Cells were lysed via sonication and centrifuged before batch binding. Lysate was bound to GST Sepharose® 4B resin (Sigma-Aldrich) overnight at 4°C with rotation. Protein was eluted by addition of 80 U of PreScission Protease (Sigma-Aldrich) in 10 mL of GST cleavage buffer (50 mM Tris-HCl, pH 7.0, 150 mM NaCl, 1 mM EDTA, 1 mM DTT) and overnight rotation at 4°C.

For further purification, proteins were buffer exchanged into AE buffer (25 mM TEA, pH 7.5, 1 mM DTT, 0 mM NaCl, 5% glycerol) for anion-exchange chromatography or GF buffer (50 mM TEA, pH 7.5, 150 mM NaCl, 5 mM DTT, 5% glycerol) for gel filtration chromatography. Proteins were applied to an anion-exchange (POROS HQ/10 column, Thermo Scientific) and/or size-exclusion (HiLoad 16/600 Superdex 200 pg, Cytiva) column and eluted using a NGC liquid chromatography system (Bio-Rad). Protein concentration was determined using Pierce Coomassie Plus Bradford Assay Reagent (ThermoFisher Scientific). Protein purity was assessed by SDS-PAGE followed by Coomassie staining (PfUbc13 > 95%, PfUbc13^{C86S} > 95%, HsUbc13 > 95%, PfUBA1 > 90%), and identity of His-tagged proteins were confirmed with HisProbe-HRP (ThermoFisher Scientific) western blotting. Protein aliquots in 25% glycerol were flash frozen using liquid nitrogen and stored at 80°C until further use.

Mass spectrometry analysis of tryptic peptides

Reaction samples consisting of 40 μM recombinant protein (PfUbc13, PfUbc13^{C86S}, or HsUbc13) in protein storage buffer were incubated with 1 mM NSC696923 or 1% DMSO at 37°C, 250 rpm for 1 h. The final volume was 50 μL. Trypsin (ThermoFisher Scientific) in 50 mM acetic acid (1:100) was then added to the samples for digestion overnight at 37°C, 250 rpm. Samples were desalted with C18 ZipTips (Millipore) per the manufacturer's instructions and separated on a C18 column using water/MeCN/formic acid in the mobile phase, a 0–100% MeCN gradient (15 min), UV detection at 280 nm, and positive ion MS (Agilent LCMS-TOF). Data shown are representative of two independent experiments.

Ubiquitin transfer visualized by western blot

In vitro ubiquitination activity assays were conducted as endpoint assays via immunoblot detection using recombinant E1 (PfUBA1) and E2 (PfUbc13^{WT}, PfUbc13^{C86S}, or HsUbc13) enzymes. E1 (100 nM) and E2 (1 μM) were incubated with ubiquitin (100 μM) in assay buffer (100 mM Tris, pH 8.0, 25 mM $MgCl_2$, 0.1% Tween), and reactions were initiated by addition of ATP (2 mM). Following 1 hour incubation at 37°C, 250 rpm, reactions were quenched with addition of SDS-PAGE loading buffer. Samples were resolved on SDS-PAGE gels and transferred to nitrocellulose membranes using a wet tank transfer system for 70 minutes. Ubiquitination activity was detected via western blot with primary anti-ubiquitin (1:1000 in blocking buffer consisting of 3% BSA in PBS with 0.2% Tween, Abcam ab7780) overnight at 4°C. Membranes were washed with PBST before incubating with Alexa Fluor 488-conjugated goat anti-rabbit secondary antibody (1:1000 in blocking buffer, Life Technologies) for 1 hour at room temperature. Blots were imaged by a BioRad Gel Imager. Data shown are representative of two independent experiments.

Fluorescence polarization assay

Reaction samples (total volume 25 μL) consisting of fluorescein-ubiquitin (100 nM, R&D Systems), ATP (5 mM), PfUBA1 or HsUBA1 (Sino Biological) (125 nM), E2 (HsUbc13^{WT}, PfUbc13^{WT}, or PfUbc13^{C86S} at 300 nM) and NSC697923 (0-32 μM, 2% DMSO) in assay buffer (50 mM Tris-HCl, pH 7.5, 140 mM NaCl, 1 mM DTT, 0.01% Tween 20) were incubated for 1 h at 37°C, 250 rpm. Reaction aliquots (15 μL) were transferred to a black bottom 384-well plate (Corning), and fluorescence polarization was measured at excitation 480 nm and emission 535 nm using an Envision (PerkinElmer) system. The percent E1∼ubiquitin in the presence of NSC697923 was calculated by normalizing data to the bound and unbound fluorescein-ubiquitin controls. Data were fit to a nonlinear curve (GraphPad Prism) to obtain the EC_{50} value for fluorescein-ubiquitin bound to E1, which was used to determine the apparent inhibitory constant (K_i). Data shown as means ± SEM, n = 2–3.

Plasmodium blood stage culture

P. falciparum (strains 3D7, Dd2, Dd2_R539T, W2) parasites were continuously cultured *in vitro* in complete medium (10.44 g/L RPMI 1640 (ThermoFisher Scientific), 25 mM HEPES, pH 7.2 (ThermoFisher Scientific), 0.37 mM hypoxanthine (Sigma), 24 mM sodium bicarbonate (Sigma), 0.5% (wt/vol) AlbuMAX II (ThermoFisher Scientific), 25 μg/mL gentamicin (Sigma)) supplemented with freshly washed human erythrocytes (Gulf Coast Regional Blood Center, Houston, TX). The parasite cultures were maintained at 2-10% parasitemia with 1% hematocrit at 37°C in a 3% O_2, 5% CO_2, 92% N_2 atmosphere. Synchronized cultures were generated by treatment with 5% (wt/vol) D-sorbitol (Sigma) at 37°C for 10 min every 48 hours.

Plasmodium blood stage inhibition assays

P. falciparum (3D7, Dd2, Dd2_R539T, W2) parasites were synchronized as described above and adjusted to 2% parasitemia and 2% hematocrit. Drug inhibition assays were performed as previously described.[53,137] Briefly, dose response curves were generated for select compounds by dispensing 100 μL of the culture into each well of a 96-well black plate (Corning), followed by administration of compounds using a HP D300 Digital Dispenser. Quinacrine at 500 nM was employed as the positive control and 0.5% DMSO as the negative control. Plates were incubated at 37°C in a 3% O_2, 5% CO_2, 92% N_2 atmosphere after drug administration. At 34 hour post-reinvasion (i.e. 72 hour after drug administration), 40 μL lysis solution (20 mM Tris-HCl, pH 7.5, 5 mM EDTA dipotassium salt dihydrate, 0.16% (wt/vol) saponin, 1.6% (vol/vol) Triton X-100) containing fresh 10x SYBR Green I (ThermoFisher Scientific) was added to each well and incubated in the dark at room temperature for 24 hour. The fluorescent signals were measured at emission at 535 nm and excitation at 485 nm using an EnVision 2105 multimode plate reader (PerkinElmer) or Spark Multimode Microplate Reader (Tecans). Data was normalized to the negative (0.5% DMSO) and positive (500 nM quinacrine) controls to obtain the relative percent parasite load. EC_{50} values were determined by fitting data to a standard dose response equation (GraphPad Prism). Technical triplicates were performed within four biological replicates for each experiment. The Z-factor ranged from 0.5-0.9.

Plasmodium liver stage inhibition assays

HepG2 cells were maintained in Dulbecco's Modified Eagle Medium (DMEM) with L-glutamine (Gibco) supplemented with 10% heat-inactivated fetal bovine serum (HI-FBS) (v/v) (Sigma-Aldrich) and 1% antibiotic-antimycotic (ThermoFisher Scientific) at 37°C with 5% CO_2. *P. berghei* ANKA sporozoites expressing luciferase were isolated from freshly dissected salivary glands of infected *Anopheles stephensi* mosquitoes (University of Georgia, SporoCore). Dose response curves were generated for NSC697923 by assessing *P. berghei* parasite load in hepatocytes as previously described.[57] Briefly, HepG2 cells were seeded (5,000 cells/well) into 384-well white microplates (Corning). After 24 hours, NSC697923 (0-100 μM) was added using a D300e Digital Dispenser

(Hewlett-Packard) before infection with *P. berghei* ANKA sporozoites (4,000 sporozoites/well). DMSO (1%) was the negative control. All samples were evaluated in triplicate and had final DMSO concentration of 1%. After 44 hours post-infection (hpi), HepG2 cell viability and parasite load were assessed using CellTiter-Fluor (Promega) and Bright-Glo (Promega) reagents, respectively, according to manufacturer's protocols. Relative fluorescence and luminescence signal was measured using the EnVision plate reader (PerkinElmer). The signal intensity of each well was normalized to the negative control to assess relative viability. Technical triplicates were performed within four biological replicates for each experiment. EC_{50} analysis was performed with GraphPad Prism.

Plasmodium liver stage size assays

HepG2 cells (4,000/well) were seeded in 384-well glass bottom plates (Cellvis-P38415HN) and allowed to recover overnight. NSC697923 (1 and 5 μM) or DMSO (1%) was added in six technical replicates prior to infection with *P. berghei* ANKA sporozoites (4,000 sporozoites/well). At 48 hpi, cells were fixed for 10 minutes with 4% paraformaldehyde (Sigma-Aldrich) at room temperature. Cells were washed three times with PBS before permeabilization with 0.1% Triton X-100 (Fisher Scientific) for 10 minutes at room temperature. After washing three times with PBS, cells were blocked with 3% BSA and 0.05% Tween-20 (Sigma-Aldrich) in PBS (blocking buffer) for 1 hour at room temperature. Cells were then probed with a goat polyclonal anti-UIS4 primary antibody (antibodies.com Cat# A121573, 1:1000) in blocking buffer for 1 hour at room temperature, washed three times with PBS, and incubated with a donkey-anti goat Alexa Fluor 488 conjugated antibody (Invitrogen Cat# A-11055, 1:400) in blocking buffer for 1 hour at room temperature. Cells were washed three times with PBS, incubated with Hoechst (1:50,000 in PBS) for 10 minutes at room temperature, and washed three additional times before acquisition.

Fixed samples were viewed on a Zeiss Airyscan 880 inverted confocal microscope (Duke Light Microscopy Core Facility) with a Märzhäuser linearly encoded x,y stage and a 63 × 1.4 NA oil-immersion plan apochromat objective. Laser illumination was via argon for 488 nm and diode for 405 nm. The fluorescence signal was collected with two photomultiplier tubes and one GaAsP detector in the following emission ranges for Hoechst (415-487 nm) and for Alexa Fluor 488 (490-570 nm). Images were acquired sequentially by line scanning bidirectionally at 0.52 microseconds per pixel with line averaging of 4 and a size of 0.044 μm x 0.044 μm with pinhole calculate to be 1 airy unit for 488 using Zeiss Zen software (version 2.3) and saved as Carl Zeiss Image files. A minimum of 50 PVs per condition per biological replicate were acquired. Image analysis was performed with FIJI. The PV size was determined by tracing and measuring the innermost signal of the PVM, excluding tubovesicular features.

Plasmodium gametocyte inhibition assays

P. falciparum gametocyte inhibition assays were performed as previously described[56] using the NF54 peg4-tdTomato reporter line.[55] Synchronously induced gametocytes were obtained following a method adapted from Fivelman et al.[138] In brief, parasites were allowed to commit to the sexual differentiation by growing at 6-8% parasitemia at 3% hematocrit. At the end of this commitment cycle, schizonts were purified using a Percoll-sorbitol gradient and then combined with fresh erythrocytes to allow for reinvasion. The newly invaded ring parasites (Day +1 of the gametocytogenesis) were cultivated at 3.5% parasitemia and 1% hematocrit with 50 mM N-acetylglucosamine to eliminate remaining asexual parasites. To observe the effect of inhibitors on early gametocytes, parasites were cultured for 6 days with 1 μM and 10 μM of NSC697923 or DMSO (control). At day +6, gametocytemia was assessed by flow cytometry (Cytek DxP11) based on the Hoechst 33342 DNA staining (375 nm laser, 450/50 emission filter) and the tdTomato fluorescent signal (561 nm laser, 590/20 emission filter). Mean tdTomato+ signal was normalized to the DMSO control and the overall minimum to determine the early gametocyte relative viability. To observe the effect of inhibitors on late gametocytes, parasites were allowed to develop for 10 days and then cultured for 2 days with 1 μM and 10 μM of NSC697923 or DMSO. At day +12, gametocytemia was assessed by flow cytometry (Cytek DxP11) based on the Hoechst 33342 DNA staining (375 nm laser, 450/50 emission filter), DilC1(5) mitochondrial potential signal staining (640 nm laser, 670/30 emission filter) and the tdTomato fluorescent signal (561 nm laser, 590/20 emission filter). Mean DilC1(5)+ tdTomato+ signal was normalized to the DMSO control and the overall minimum to determine the late gametocyte relative viability. Technical duplicates were performed within three biological replicates for each experiment. The effect of SGI-1027 at 1 μM and 10 μM was used as a positive control in both early and late gametocyte inhibition assays.[56]

Evaluation of K63-Ub and K48-Ub levels

P. falciparum 3D7 was cultured until parasitemia reached 10-20% at 1% hematocrit and then 1 μM NSC697923 or 0.1% DMSO (negative control) was added. After 48 hours, parasites were separated from erythrocytes via lysis with 0.03% saponin in PBS on ice for 15 min. The parasite pellets were washed with ice-cold PBS until supernatant no longer appeared red. Pellets were then flash frozen in liquid nitrogen and stored at −80°C until lysis. Parasite lysate was generated by pellet resuspension in parasite lysis buffer (4% SDS, 0.5% Triton X-100, 50% PBS) and sonication. Cellular debris was removed by centrifugation. Parasite proteins were resolved on SDS-PAGE gels and transferred to nitrocellulose membranes using the Trans-Blot Turbo Transfer system (Bio-Rad). The membranes were blocked with 3% BSA in PBST (0.2% Tween 20) at room temperature for 1 hour. The membranes were then probed with 10 mL blocking buffer with K63-linkage specific anti-ubiquitin (Abcam ab179434) at a 1:1000 dilution overnight at 4°C. Membranes were washed three times with PBST before incubating with Alexa Fluor 488-conjugated goat anti-mouse antibody (ThermoFisher Scientific) at a 1:1000 dilution for 1 h at room temperature. After three washes with PBST, fluorescence signals were detected using a ChemiDoc MP imaging system (Bio-Rad). Membranes were stripped with Restore Western Blot Stripping

Buffer (ThermoFisher Scientific) per the manufacturer's instructions. Membranes were reblocked, then probed with K48-linkage specific anti-ubiquitin (1:1000 in blocking buffer, Abcam ab140601) overnight at 4°C. Membranes were washed before incubating with Alexa Fluor 488-conjugated goat anti-rabbit antibody (ThermoFisher Scientific). Signal intensities from three biological replicates were normalized to Ponceau S total protein stain (ThermoFisher Scientific) and quantified using ImageJ (Fiji).

K63-TUBEs enrichment of *Plasmodium* proteins

P. falciparum 3D7 was cultured as described above until ring stage parasitemia reached 10-20% at 1% hematocrit and then 1 μM NSC697923 or 0.1% DMSO (negative control) was added. After 48 hours, parasites were separated from erythrocytes via lysis with 0.03% saponin in PBS on ice for 15 min. The parasite pellets were washed with ice-cold PBS until supernatant no longer appeared red. Pellets were then flash frozen in liquid nitrogen and stored at −80°C until lysis. Parasite lysate was generated by pellet resuspension in TUBEs lysis buffer (100 mM Tris-HCl, pH 8, 150 mM NaCl, 5 mM EDTA, 1% NP-40, 10% glycerol, 10 μM NEM, 10 μM PR619, 1 cOmplete™ tablet) and sonication. Cellular debris was removed by centrifugation and protein concentration was determined using Pierce Coomassie Plus Bradford Assay Reagent (ThermoFisher Scientific). Parasite supernatant was added to washed K63-Ub TUBEs magnetic resin or negative control magnetic resin (LifeSensors) in a ratio of 1:100 (mg protein mass: μL volume of resin). Lysate was incubated with TUBEs resin for 2 hour, rotating at 4°C. TUBEs were then spun down, magnetized, washed three times with PBST and bound proteins were eluted by addition of 50 mM TEAB with 5% SDS and heating at 100°C for 10 min.

The lysates generated from TUBE enrichment were subjected to a previously described filter-aided sample preparation (FASP) protocol.[139] Samples (~10 μg) were added in Amicon 0.5 mL 10 kDa MWCO filter units and washed three times with 8 M Urea in 0.1 M Tris-HCl, pH 8.5. Samples were then treated with 5 mM TCEP for 1 hour followed by 20 mM MMTS for 15 min at room temperature. After alkylation, the filter units were washed 3 times with 0.1 M TEAB buffer and 1 μg of trypsin was added to each filter for trypsinization. Peptides were eluted by 3 washes of 500 mM NaCl, desalted with Macrospin C18 columns, and dried before LC-MS/MS analysis.

LC-MS/MS analysis

Samples were reconstituted with 1% TFA and 2% ACN such that the final peptide concentration was ~1 mg/mL. LC-MS/MS analyses were performed on a Thermo Orbitrap Exploris 480 with a ThermoEasy nano LC 1200. Samples (~1 μg) were injected onto the column and resolved using a nanoViper 2Pk C18, 3 μm, 100 Å, 75 μm × 25 cm analytical column (ThermoFisher Scientific). The samples were analyzed in a gradient going from 3.2% to 28% ACN in 90 min, 28% to 32% ACN in 5 min, and 32% to 80% ACN in 5 min before the column was washed with 80% ACN for 5 min. The MS1 acquisition was performed with 120000 resolution, 375-1500 *m/z* range, and 300% normalized Automatic Gain Control (AGC) target. The acquisition window between two MS1 scans was 2.5 s, and the isolation window was set as 1.2 *m/z* for selecting precursor ions for data dependent acquisition (DDA). The high-energy collision-induced dissociation (HCD) was performed with 36% HCD normalized collision energy, and the MS2 scan was performed with a resolution of 45000, 300% normalized AGC target, and 105 ms of maximum ion injection time. Each peptide sample was analyzed in triplicate by LC-MS/MS.

Label-free quantitation data processing

The raw data acquired from LC-MS/MS analysis was searched using Thermo Proteome Discoverer 2.3 against the *P. falciparum* 3D7 isolate proteome from UniprotKB (Uniprot proteome ID: UP000001450). The data was searched with fixed MMTS modification of cysteine; variable oxidation of methionine; variable deamidation of asparagine and glutamine; and variable acetylation of the protein N-terminus. Trypsin was used as the enzyme, and the number of missed cleavages allowed was set to 2. The other software settings were set to default.

Only parasite proteins identified by two unique, high-confidence peptides (FDR < 1%) in both biological replicates were considered for quantitative analysis. In the quantitative analysis, two normalization steps were performed. First, a normalization factor determined from the ratio of summed raw quantified ion intensities from DMSO-input/NSC697923-input was calculated. This normalization factor was applied to the quantified ion intensity for each protein in the input NSC697923-treated sample. Then, the DMSO-input/NSC697923-input ratio was calculated for each protein and applied to the NSC697923-treated K63-enriched proteins to normalize for protein expression changes. Subsequently, a normalization factor to account for technical variabilities was calculated from the ratio of summed quantified ion intensities from DMSO-K63 enriched/NSC697923-K63 enriched proteins and applied to the quantified ion intensities of each protein in the NSC697923-K63-enriched sample. Imputation of missing values with the minimum normalized quantified ion intensity of each group was performed. Normalized fold-change values were calculated (NSC697923-K63 enriched/DMSO-K63 enriched) and log2-transformed per replicate for each protein. The Gaussian distribution fit of the normalized average log2 fold-change values was calculated (R^2 = 0.88) in Graphpad Prism (Figure S3C). Similarly, normalized abundance ratios were calculated from the quantified ion intensity for each protein from pulldowns with a negative control resin (negative control/input). Proteins with K63-TUBEs -log2 fold-change >0.50 and negative control fold-change <0.50 in both biological replicates were compiled (31 hit proteins) for Gene Ontology analyses in PlasmoDB and REVIGO with visualization in Cytoscape[135,136] and further comparative analysis with three additional *P. falciparum* ubiquitinated proteins datasets.[13,60,61] The Proteome Discoverer protein summaries output, filtered protein intensities, calculated log2 fold-change values, and hit overlap analysis are detailed in Tables S1-S3.

O-propargyl puromycin incorporation assay

P. falciparum 3D7 was cultured as described above until trophozoite parasitemia reached 10% (i.e. 24 hours post-invasion) at 1% hematocrit. Then, DMSO (0.1%), NSC697923 (1, 5, 10 μM), WR99210 (0.1, 0.5, 1 nM), or bruceantin (5 nM) was added, or heat shock treatment (42°C) was begun. After 4 hours, o-propargyl puromycin (Click Chemistry Tools) was added (1 μM). After 2 hours, parasites were separated from erythrocytes via lysis as described above. Copper(I)-catalyzed alkyne-azide click reaction was performed with parasite lysate by the addition of $CuSO_4$ (1 mM), TBTA (100 μM), TCEP (1 mM), and Alexa Fluor 488 Azide (1%) (ThermoFisher Scientific). Parasite proteins were resolved on SDS-PAGE gels, and in-gel fluorescence signals were detected using ChemiDoc MP imaging system (Bio-Rad). Coomassie protein stain was used to measure protein loading. Signal intensities were normalized to Coomassie total protein stain (ThermoFisher Scientific) and quantified using ImageJ (Fiji). Analyses were performed from three independent experiments.

QUANTIFICATION AND STATISTICAL ANALYSIS

GraphPad Prism 10 software was used for analysis of data. The sample size, standard error, significance, and statistical test employed for analysis are noted in respective figure legends.